August 2014

Microfluidic Device Integration of Electrostatic Corral Trapping Systems

Alaknanda Amin
University of Wisconsin-Milwaukee

MICROFLUIDIC DEVICE INTEGRATION OF ELECTROSTATIC CORRAL TRAPPING SYSTEMS

by

Alaknanda P. Amin-Patel

A Thesis Submitted in

Partial Fulfillment of the

Requirements for the Degree of

Master of Science in Chemistry

at

The University of Wisconsin-Milwaukee

August 2014

ABSTRACT

MICROFLUIDIC DEVICE INTEGRATION OF ELECTROSTATIC CORRAL TRAPPING SYSTEMS

by

Alaknanda P. Amin-Patel

The University of Wisconsin-Milwaukee, 2014
Under the Supervision of Jörg C. Woehl

This thesis describes the development, characterization, and application of the microfluidic device integration of electrostatic corral trapping systems. Optical traps or “laser tweezers”, which are capable of trapping microscopic dielectric particles through the production of steep electromagnetic field gradients, have been significant in the development of the field of biophysics and the manipulation of microscopic objects. This method of trapping unfortunately has a fundamental size limitation, making it incapable of trapping molecular-scale objects. We have developed a new tool for the trapping and manipulation of nanoscale objects including single molecules, the corral trap, which has distinct characteristics that set it apart from other trapping techniques. In order to increase the versatility of this new trapping tool, steps have been taken to integrate corral traps in a microfluidic cell. The production of such integrated devices based on optical lithography techniques will be presented in detail. Corral trapping in microfluidics device is expected to have important future applications in areas such as biomedical assays, ultra-sensitive biochemical analysis, and

DNA manipulation and screening. Novelty: A novel method for the trapping of single molecules has been successfully used for the trapping of single ssDNA molecules.

TABLE OF CONTENTS

LIST OF FIGURES

LIST OF TABLES

LIST OF ABBREVIATIONS

ABEL	Anti-Brownian Electrokinetic Trap
ADC	Analog-to-Digital Converter
BHF	Buffered Hydrofluoric Acid
BOE	Buffered Oxide Hydrofluric Acid
CCD	Charge Coupled Device
DIC	Differential Interference Contrast
DNA	Deoxyribonucleic Acid
EDTA	Ethylenediaminetetraacetic Acid
EMCCD	Electron Multiplying Charged Coupled Device
GC	Gas Chromatography
HF	Hydrofluoric Acid
HMDS	Hexamethyldisilazane
NICHROME	Nickel-chromium
nt	Nucleotide
PDMS	Poly(dimethylsiloxane)
PMMA	Poly(methyl methacrylate)
PVD	Physical Vapor Deposition
PR	Photoresist
ssDNA	Single stranded Deoxyribonucleic Acid
TBE	TRIS Boric Acid - EDTA buffer
TIFF	Tagged Image File Format

TRIS	Tris(hydroxymethyl)aminomethane
UV	Ultra-Violet

LIST OF SYMBOLS

n_b	Index of Refraction of the Medium
r	Radius
m	Medium
ω_o	Size of Beam Focal Spot
t	Thickness
m	Mass
ρ	Density
d	Distance
S_0	Ground State
C	Capacitance
V	Voltage
pH	Negative logarithm of the hydrogen ion activity
f	Focal length
L	Tube length
l	Length
R	Resistance
κ	Trap stiffness
I	Intensity
λ	Wavelength
I	Current
E	Electric Field

ACKNOWLEDGEMENTS

I enjoyed doing research at UWM, and this wasn't because of the lovely view from my office. I enjoyed it because I shared the time with wonderful supportive adviser and friends. I first wish to express my gratitude to my advisor Dr. Jörg C. Woehl, whose expertise, understanding, and patience, added considerably to my graduate experience. In addition to this, I like to thank Dr. Elizabeth Hoppe, Dr. Heather Owen and Dr. Woo-lin Chang for all your support in every way I needed. Thanks for taking time to listing and advising. I would like to thank the members of my thesis committee, Dr. Geissinger and Dr. Pacheco.

The One Molecule Lab is populated by great scientists and friendly people who gave great advice and enjoyed working are Taher Ababneh, Bradley Moran, Xavier Udad, and Quintus Owen. I especially like to thank Dr. Christine Carlson, who has helped me tremendously in research as well as life lessons. She has been with me for every step of my research as an inspiration, mentor and friend. Thank you all for your support and good memories to look back.

Alaknanda Amin-Patel

Milwaukee, WI

August 2014

This thesis is dedicated to my Parents, Ashwin and Jyotsana Patel, all they wanted was for me to find my dreams and be happy.

I also want to dedicate this work to the numerous people who have helped me reach this point in my life. My mother-in-law Hemlatta and father-in-law Rameshchandra Amin, who have helped me tremendously thru out Graduate School and without them this would have not been easy journey. To my sisters Avanti, and Nilam Patel, who were there with me all thru my life and can depend on them for anything. To my two beautiful and wonderful children Preet and Meera Amin, all this has been for you. Finally to my best friend, my husband, Parag Amin; I would have crumbled on many occasions if it were not for your constant unconditional support and love.

Chapter 1

Introduction

1.1 Organization of the thesis

Nanoscience is the study of the phenomena and manipulation of materials at atomic, molecular and macromolecular scale. Nanotechnology represents for many researchers the great "challenge of 21st century"[46]in medicine with regard to three key areas diagnosis, treatment and regenerative medicine. There is wide interest in manipulation of nanoscale objects for the fabrication of nanosensors and nanodevices.

The work performed in this thesis focuses on trapping single molecules and the fabrication of an electrostatic corral trapping system into a microfluidic device. Christina Carlson has successfully demonstrated corral trapping of 800 nucleotide (nt)ssDNA[10], 2 μm, and 20 nmpolystyrene beads[10]. In this thesis electrostatic corral trapping of 600 nt ssDNA and fabrication of integrated electrostatic corral trapping in a microfluidic device will be demonstrated.

Chapter 1 presents the theory and experimental designs for the most significant approaches to the trapping of microscopic particles and molecular-size objects. Chapter 2 is based on electrostatic corral trapping theory. Chapter 3 presents materials, lab setup, instrumentation, laser and microscope setup for fabrication of corral traps. Chapter 4 details the fabrication of microfluidic device. Chapter 5 presents the trapping of 600 nucleotide (600 nt) ssDNA. Chapter 6 consists of conclusion and future direction of the trapping of objects in electrostatic corral integrated in a microfluidic device.

1.2 Optical tweezers

Ashkin and co-workers developed in 1986 what is now known as optical tweezers or laser tweezers, demonstrating for the first time[1] optical trapping of dielectric particles by a single-beam gradient force trap. Trapping was observed for particles ranging in size from 10 μm to 25 nm in water[1]. The single beam gradient trap has since become an essential tool for research in biology, chemistry and biophysics. In the field of biological chemistry and biophysics it is important to be able to manipulate particles in the micron-size regime without damaging them. Optical tweezers prove very useful for this because not only can they manipulate small particles very specifically, but using infrared light, they can do so without causing damage[1].Optical tweezers have been used to trap dielectric spheres[5], viruses[4], bacteria[4], living cells[1], and even strands of DNA[11].

Optical tweezers use extremely small forces resulting from a highly focused laser beam to manipulate nanometer and micron-sized dielectric particles. The beam width of a focused laser beam changes as a function of the axial distance and, at the narrowest point, is called the beam waist. In the beam waist, laser beam exhibits a very strong electric field gradient. A dielectric particle in an electric field gradient will move towards the point with the strongest electric field gradient. This is expressed by the following equation,

$$\vec{F}_{\text{grad}} = -\frac{n_b^3 r^3}{2}\left[\frac{m^2 - 1}{m^2 + 2}\right]\vec{\nabla} E^2$$

where, r is the particle radius, m is the effective refractive index of the sphere relative to that of the medium, n_b is theindex of refraction of the medium, and E the electric field of the incident light.

However, gradient force is not the only force acting on the particle. As the dielectric particle is hit by a laser beam, photons get scattered or absorbed by the particle and their momentum is transferred to the particle. This applies a force to the particle in the direction in which the laser is propagating. This force is called scattering force, and it causes the particle to move a position slightly beyond the beam waist in direction of the laser propagation[1, 6] in figure 1.1.

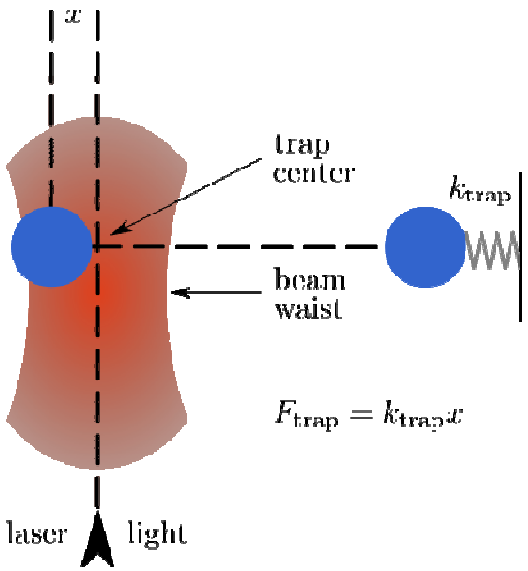

Figure 1.1.Dielectric particle is pushed to the center of the beam and as the laser light is propagating upstream, it is pushed slightly higher than the beam waist. In this situation the applied force to the particle is linearly dependent of its displacement from the trap center and it can be modeled as a simple spring system (This figure was taken exactly from Wikipedia)[6].

The scattering force points in the direction of the incident light and is proportional to the intensity.

$$\vec{F}_{\text{scat}} = \frac{I_o 128\pi^5 r^6}{c3\lambda^4} \left[\frac{m^2 - 1}{m^2 + 2}\right]^2 n_b$$

where, r is the radius of particle, m is the refractive index ratio between that of the particle and that of the medium, I_0 is the intensity of incident light, c is the speed of light in vacuum, λ is the wavelength in of the incident light, and n_b is the index of refraction of the medium [7]. Optical trapping behavior depends on relative comparison of the particle size and the wavelength of used laser. Simple ray optics can be used whenever the dimensions of the particle are much greater than the wavelength. If the trapped particle is much smaller than the wavelength of the trapping laser, the conditions for Rayleigh scattering are satisfied[1]. For the trapping to work the force gradient must be greater than the force pushing the dipole out of the field scattering[7]; therefore, the ratio of the gradient force to the scattering force must be greater than unity. As long as this condition is satisfied a single laser beam can be used to trap a particle in the Rayleigh regime.

$$\frac{\vec{F}_{grad}}{\vec{F}_{scat}} > 1$$

For the gradient force to overcome the scattering force and Brownian force, two parameters, have to be consider: particle size and optical intensity. For smaller particle higher optical intensity is required, which can lead to optical damage. The optical trap has high positioning accuracy and is a well-established technology, but is limited by size of the particle being trapped.

1.3 Anti-Brownian electrokinetic trap (ABEL) trap

The Anti-Brownian Electrokinetic (ABEL) trap eliminates the Brownian motion of one object in solution, allowing detailed examination of its properties.

ABEL trap gives scientist new technique to nano world. The first demonstration of this trap was in 2005, 100 years after Einstein's annus mirabilis, in which he addressed the fundamental thermal mechanisms for Brownian motion[45].

ABEL trapping works by monitoring the Brownian motion of the fluorescent particle and applying a time-dependent feedback voltage to the solution, so that the electrokinetic drift exactly cancels out the Brownian motion[8]. ABEL trap is non-invasive, gentle to handle biological molecules and can trap objects smaller than laser tweezers. The ABEL trap does not have the positioning accuracy of the optical trap since it is limited by the resolution of the imaging system. The electrophoretic trapping can only trap one particle at a time since the counteraction of this particle's Brownian motion is at the heart of the method, which makes it impossible to cancel the (random) Brownian motion of a second object at the same time.

1.4 The electrostatic corral trap

The electrostatic corral trap was developed in the Woehl Lab and first successfully demonstrated by Christine A. Carlson in 2010[9]. It is a novel tool for trapping micro- and nano- scale objects. The function of the corral trap is based on pure electrostatic charges which create a stable potential energy well for trapping[9]. Once an object is trapped, the electrostatic corral trap doesn't need information about its location and does not require a feedback loop.

The electrostatic corral trap operates by generating a circular potential energy well shown in figure 1.2[10], due to charges at the rim of the circular pattern. Such a pattern can be fabricated by deposition of thin metal film on a substrate

with circular, uncoated areas (“holes”). By applying a potential to the metal film, accumulation of charges occurs at the metal rim of the circular holes, acting like an invisible fence.

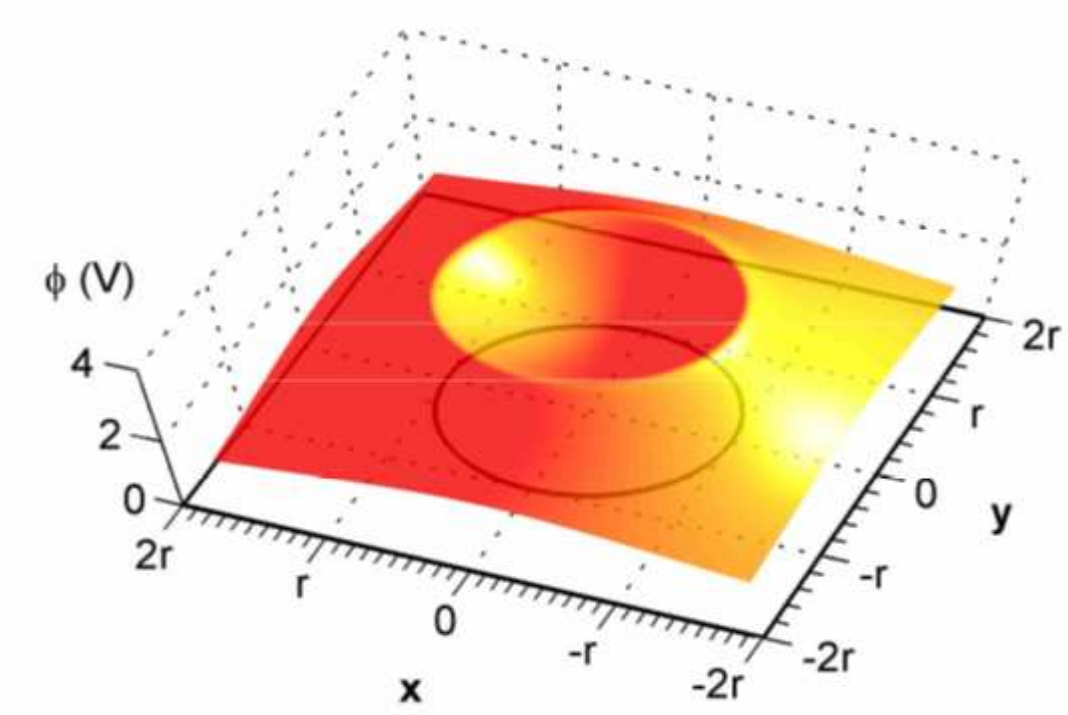

Figure 1.2. Electrostatic potential above a circular charge distribution (black ring in the xy plane; linear charge density: 0.3 e/nm; radius r) in a parallel plane at distance r/5[10] (This figure is taken from Christine Carlson’s thesis with her permission).

The electrostatic corral is fabricated using conventional micro-patterning techniques, which will be discussed in detail in Chapter 3 to create a circular hole patterned into a thin metal film which has been evaporated onto a substrate. By charging the thin metal film a potential energy well can be created at the location of the micro-patterned circular hole due to the accumulation of charges at the rim of the circular hole (Figure 1.3).The trapped object can only be released by turning off the voltages. Electrostatic corral traps can be integrated in a

microfluidic device for trapping and manipulating single molecules such as viruses, proteins, beads and DNA in solution.

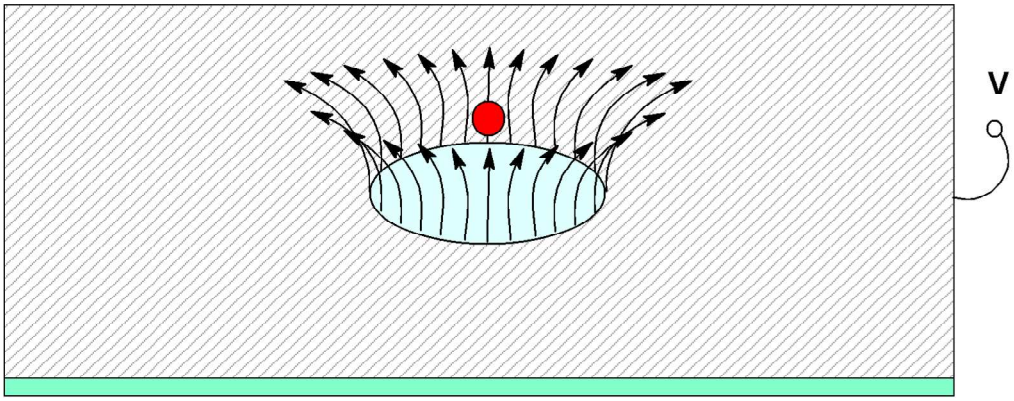

Figure 1.3.The trap consists of a glass support covered with a thin layer of metal. Patterned into the metal is a micron-scale hole. When a potential is applied to the thin metal film an electric field is produced through the accumulation of charges on the edge of the hole[10] (This figure is taken from Christine Carlson's thesis with her permission).

1.5 Microfluidic device

Microfluidics is the science that deals with the flow of liquid inside channels where at least one dimension of the channel has micrometer size. Microfluidics has first emerged in 1977[13] at IBM, where ink jet printer nozzles were developed and were used in gas chromatography (GC) in 1979[12]. Since then microfluidics has shown various applications in fields of chemistry, biochemistry, engineering, physics, nanotechnology and biotechnology. Microfluidics is used to study the behavior, precise control and manipulation of particles in fluid channel that are geometrically sub-millimeter scale (nL, pL, fL). The behavior of the particles in fluids at the micro scale can differ due to surface tension, energy dissipation and fluidic resistance dominating the system.

1.5.1 Application areas

Microfluidics has large number of applications, such as in pharmaceuticals and biotechnology. Pharmaceutical vaccines, cancer, antibiotics, and injectable as well as inhalable steroids can be studied with microfluidics[14, 15]. Biotechnology applications are quantification of E. coli, yeast, algae, bacteria, plant, insect, fungi. Benefits of microfluidics use of pharmaceutical and biotechnology applications are particle size reduction, uniform particle size distribution, reliable scale up[14, 16], and rapid cell rupturing[14, 16]. In the field of energy microfluidics has applications in fuel cells, batteries, photovoltaics, biodiesel with benefits ranging from reducing reliance on fossil fuels, never degrade or emit minimal greenhouse gases[14, 16].

1.5.2 Manufacturing methods

The manufacturing capability of microfluidic devices depends upon material selection. Materials used for fabrication of microfluidics device are wet silicon etching(chemical removal of layer), dry silicon etching (plasma assisted etching) , lithography (using series of chemical reactions), and laser ablation (bond-breakage by a pulsed UV source). Commonly used materials in microfluidics manufacturing are low fluorescence Schott borofloat glass, Corning 0211 borosilicate glass fused silica, quartz silicon, PMMA, SU-8 photoresist, poly(dimethylsiloxane) (PDMS), and other more materials[17, 18, 19].

1.5.3 Bonding techniques

A microfluidic chip consists of a set of micro-channels etched or molded into a material. The micro-channels forming the microfluidic chip are bonded

together with substrate in order to achieve a desired function. Bonding remains a critical step in any fabrication process because of different materials being bonded together. Strong bonding in microfluidic devices is essential for good seal so that no leakage of solution occurs. Bonding methods can be divided into mainly two categories: direct wafer bonding or bonding with intermediate layers (Indirect wafer bonding) [20, 21].

Direct wafer bonding refers to flat and clean wafers of almost any material brought into contact at room temperature and bonded together chemically or by attraction of each other due to van der Waals forces[20, 21]. Direct wafer bonding can be due to fusion bonding, which means bonding between two parts of the same materials and an anodic bonding, which means bonding between different materials[22]. Fusion bonding is achieved on a flat clean substrate washed with piranha solution and immersed in ammonium hydroxide, and then two wafers are pressed together for few hours[22]. Anodic bonding is done by contacting the substrates together, heating, bonding by the application of an electrostatic field and then cooling down[22].

Indirect wafer bonding has two categories; PDMS bonding and SU-8 bonding. PDMS has O_2 plasma treatment before bonding and bonding occurs due to siloxane bonds between two wafers[23]. SU-8 bonding is done by cleaning substrate using piranha solution; spinning a layer of SU-8 photoresist onto the substrate and sealing the cross-link SU-8 structures to a second cleaned substrate[23]. These bonding techniques can be used for materials such as silicon, glasses, polymers, ceramics, and metals. In this thesis indirect wafer bonding is used to make microfluidic devices and will be discussed in detail in Chapter 4.

Chapter 2

Electrostatic Trapping Theory

2.1 Overview

In this chapter electrostatic corral trap theory is presented. The chapter begins with a fundamental explanation for the trapping mechanism. Next, the shape of the potential well produced by the application of an electric potential to the corral trap is investigated and expression for the theoretical trap stiffness is given. The chapter concludes with a discussion of capacitance measurement.

2.2 Fundamental idea of electrostatic corral trapping

The basic idea of corral trapping lies in the action of purely electrostatic forces on charged particles. The idea of the corral trap is illustrated with the figure 2.1. In the figure two positive charges Q_1 and Q_2 are shown at fixed spatial positions. The particle q in figure 2.1 also caries positive charge and is allowed to move freely within the plane. The force on q is the net Coulomb force repelling the charged particle from the fixed charges. If q lies on the perpendicular bisector axis, then the net force has no lateral component. On other hand if q shows a lateral displacement from the bisector axis, the symmetry is broken and the net force acquires a lateral force component (shown in red) that pulls the particle back to the null position. The lateral restoring force gradually increases with increasing lateral movement and, for large lateral displacements beyond one of the fixed charges, finally changes direction repelling the particle away from the null position.

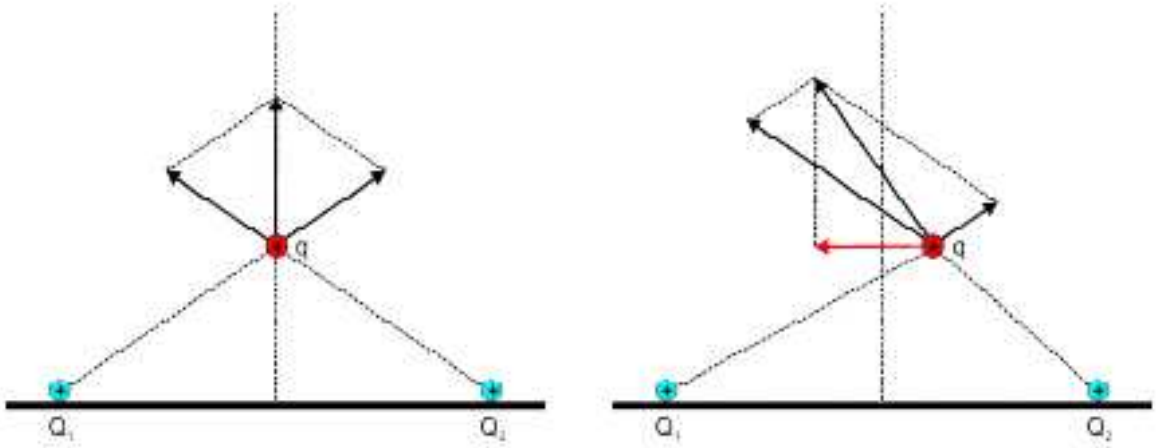

Figure 2.1. One-dimensional analog of the corral trap. In the symmetric case shown left, the force exerted by two identical fixed charges $Q_1$and Q_2on the charge q does not have any lateral component (null position). A small lateral displacement of the charge, however, leads to a restoring force with a lateral component (red arrow) that pulls the particle back to the null position (right) (This figure is taken from Christine Carlson's thesis with her permission).

2.3 Ring of charge

Imagine a thin metal film with circular holes on a glass substrate that has been fabricated by thermal evaporation. When the thin film is charged, the rim of metal around such a hole exhibits a very high surface charge density due to the small surface curvature at the rim. The accumulation of charges along the rim mimics the intended charge geometry, for corral trapping.

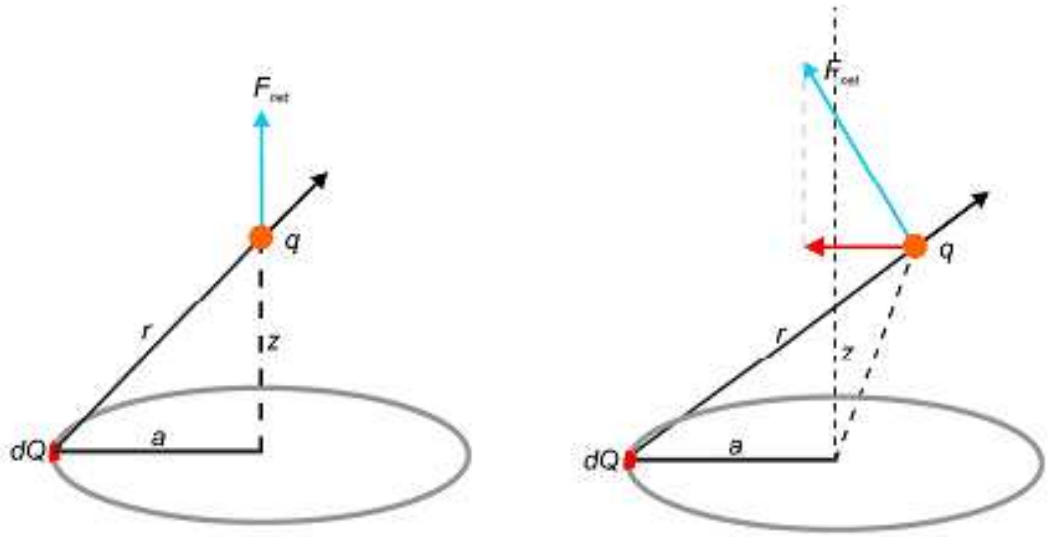

Figure 2.2. Circular charge distribution. The net electrostatic force due to each element of charge, dQ, in a circular charge distribution can be calculated from simple electrostatics. (Left) The net Coulombic force acting on a charged particle, q, on the axis of symmetry is solely comprised of an axial force (blue). (Right) If the charged particle is displaced from the axis of symmetry the net Coulombic force (blue) now contains both an axial and lateral component (red) (This figure is taken from Christine Carlson's thesis with her permission).

The potential a charged ring can be found by considering the ring as a line of charge bent into shape of a ring and dividing the ring into equal elements of length, *dx*. Each *dx* contains a charge *dQ* and each element of charge (*dQ*) can be considered as a point charge which contributes to the net electrostatic potential acting on the charged particle *q*. The electrostatic potential that *q* experiences due to the charge element *dQ.*

$$d\phi = \frac{k \cdot dQ}{r}$$

When, $r = \sqrt{a^2 + z^2}$, we are dealing with a special case, namely the one depicted in Fig. 2.2 on the left, where the charged particle is on the bisector axis, where.

$$d\phi = \frac{k \cdot dQ}{\sqrt{a^2 + z^2}}$$

The total electrostatic potential can be found by integrating around the circumference of the ring, (adding the contribution from each element of charge),which in this special case results in

$$\oint d\phi = \frac{k}{\sqrt{a^2 + z^2}} \oint dQ$$

The electric potential when the particle is on the axis of symmetry is therefore:

$$d\phi = \frac{k \cdot Q}{\sqrt{a^2 + z^2}} = \frac{k \cdot Q}{r}$$

Where Q is the total charge of the ring.

The above equation, only gives the electrostatic potential on the bisector axis. To calculate the figure below, the more general equation (with the “r” in it), has been used directly. A simulation of the electrostatic potential of the circular charge geometry has been produced and results of these calculations are shown in Figure 2.3 for the xz plane, where, z is the axial direction.

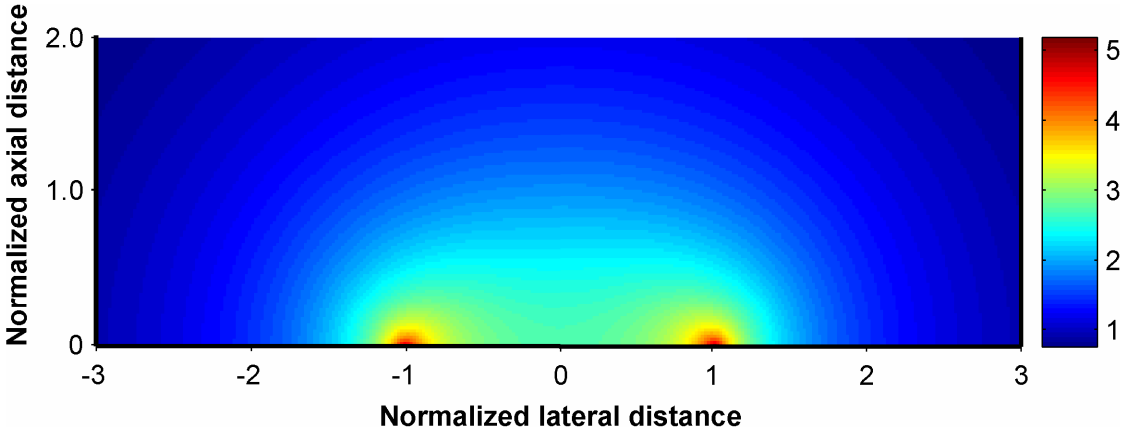

Figure 2.3. Electrostatic potential map. Simulation of the electrostatic potential (in V) of a corral trap (normalized to the trap radius), all distances are expressed as

multiples of the trap radius. (This figure is taken from Christine Carlson's thesis with her permission).

In figure 2.3 a linear charge density of 0.3 elementary charges per nm for the uniform circular charge distribution along the circumference of the trap is assumed. Approximately 10000 elementary charges were placed on a micro scale corral with a radius of 5 μm. It can be seen in figure 1.2 that the charge distribution generates a corral shaped, axis symmetric potential well. The potential well has a barrier height that decreases with the increasing axial distance.

The question still remains, whether the assumed linear charge density is a realistic estimate for typical applied voltages. The problem is how to best model the charge accumulation on the metallic ring.

2.4 Capacitance

In order to estimate the charge on the metallic ring the capacitance of the charge distribution needs to be determined. The capacitance (C) of an electrostatic system is defined as the ratio of the quantity of charge Q separated by the applied potential difference or voltage (V).

$$C = \frac{\mathrm{Q}}{\mathrm{V}}$$

The set up used for capacitance measurements of a10 nm thick Nickel-Chromium (NiCr) and Gold-Palladium(AuPd) metal film with embedded corral traps and coved by ssDNA sample solution is shown in figure 2.4. A capacitance tester was made in house by Daniel Shurilla. A coverslip with corral traps, power

supply and oscilloscope were attached to capacitance tester by thin wire as shown in figure 2.4. The oscilloscope measured the decay of the potential of the coverslip (-30V were applied by power supply through capacitance tester) once the device was connected to ground. Charge and discharge were controlled by the two red and gray buttons on capacitance tester.

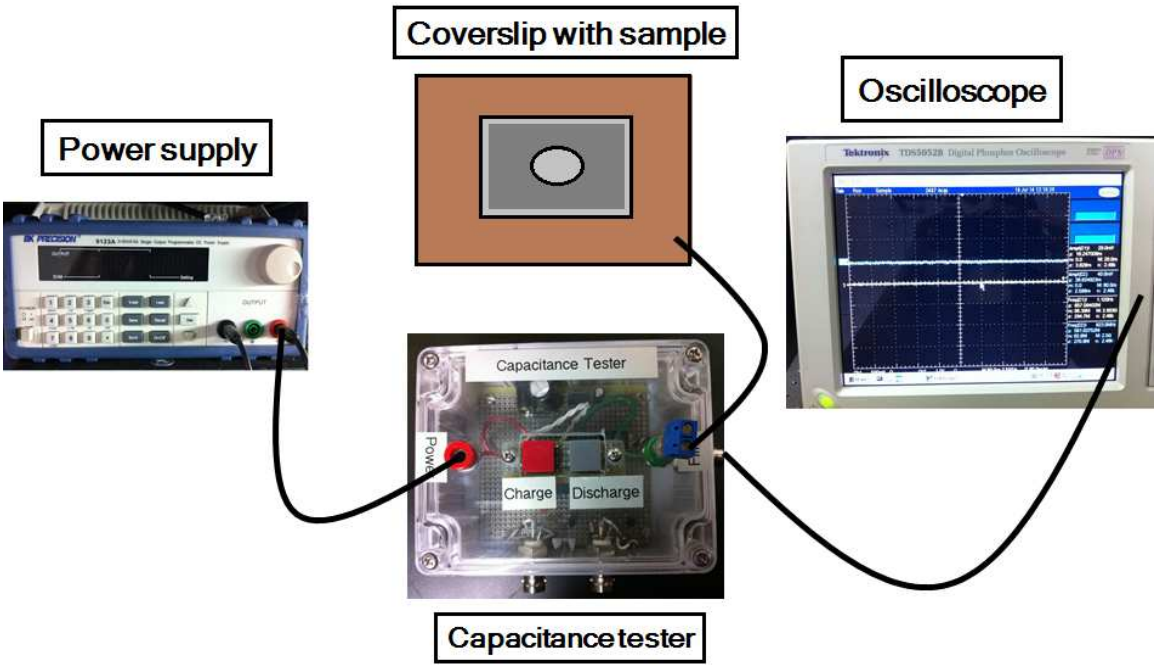

Figure 2.4. The set up used for capacitance measurements.

Ohm demonstrated that there are no perfect electrical conductors through a series of experiments in 1825 and every conductor he tested offered some level of resistance *R*. Ideally, the resistance can be expressed as a linear function of the applied voltage *V*, $R = \frac{V}{\mathrm{I}}$ with the current defined by $I = -\frac{dQ}{\mathrm{dt}}$ where *I* is current, *V* is applied potential, *R* is resistance and *t* time. This means that the discharge current of a capacitor in series with a resistance is given by

$I = -\frac{dQ}{dt} = \frac{V}{R} = \frac{Q}{CR}$, which can be integrated to result in the following expression:

$$\frac{dQ}{Q} = -\frac{1}{CR}dt$$

$$Q = Q_0\, e^{-(1/CR)t},$$

$$V = V_0\, e^{-(1/CR)t},$$

$$I = I_0\, e^{-(1/CR)t}$$

The capacitances determined from the experiments resulted in an average value of 1.6 x 10^{-12}F; the results are not what were expected compared to result reported by Christine Carlson[10]. This issue is still under investigation; higher capacitance measurements may be due to surface properties of the metal coating itself as the thermal evaporation conditions had dramatically changed since the early experiments. The evaporator has been changed as well as there is currently no method to accurately measure the film thickness, which is why we are setting up a new evaporation system with thickness monitor so that these effects can be studied more systematically.

2.5 Trap stiffness

Stiffness is measurement of how tightly a particle is held inside a trap. In a Hookean system, the force exerted upon the particle is proportional to the distance of the particle from the potential minimum, as represented by,

$F = -\kappa x$

where, x is the position of the particle relative to the center of the trap, and the parameter κ is referred to as the trap stiffness. In our experiments stiffness depends on the potential applied, the greater potential applied the stronger the hold on the trapped molecule. This has been investigated in great detail in Christine Carlson's thesis[10].

Chapter 3

Materials and Experimental Methods for Fabrication of Traps

3.1 Materials for micro-scale traps

This chapter focuses on the fabrication of corral traps based on an experimental protocol established by Christine Carlson[10].A solid substrate used for fabrication of the micro-scale traps is 25 mm x 25 mm traditional glass coverslip with a thickness of 0.16 mm - 0.19 mm (VWR 48366-249). The glass substrate was cleaned by highest grade solvents to ensure minimum impurities are:

- Acetone (VWR BJ010-4; HPLC grade)
- Methanol (Sigma-Aldrich 650609; HPLC grade)
- Isopropanol (Sigma-Aldrich 650447; HPLC grade)
- Toluene (Fisher Scientific 095606; HPLC grade)
- Ultrapure water with a resistivity of 18.3 MΩ·cm was used for all aqueous preparations (Sartorius Arium 611V)

10.0 µm polystyrene beads with a coefficient of variation of less than 4% (Microspheres-Nanospheres 100243-05, # C-PS-10.0) were used as a mask to make traps on 25 mm x 25 mm glass substrates. Thin metal film was formed by thermally evaporating a small amount of metal on the substrate using an Edwards coating system (Edwards Vacuum, E306A). Single strand tungsten filaments (Ted Pella 27-19) and single strand tungsten baskets (Ted Pella 72-1) were used to hold metal inside the evaporator. The metals used for thermal evaporation are:

- Gold: ρ=19.3 g/cm^3, mp=1062°C (VWR AA14722-FF)

- 60:40 Nickel-Chromium (Nichrome): ρ=8.5 g/cm^3, mp=1395°C (Kurt J. Lesker, EVMNICR500)
- 60:40 Gold-Palladium: ρ=16.4 g/cm^3, mp=1552°C (Ted Pella 22-2)
- Aluminum: ρ=2.7 g/cm^3, mp=660.32°C (Ted Pella 20/10-1)
- Silver: ρ=10.49 g/cm^3, mp= 961.78°C (Alfa Aesar B06S033)

3.2 Fabrication of traps

So far only traps fabricated using the shadow evaporation method have been used in trapping experiments, although lithographically patterned traps could be used as well. The method used to fabricate traps has been established by Christine Carlson[10] and same method has been followed in this thesis.

3.2.1 Shadow evaporation

Shadow evaporation was first developed by T. Fulton and G. Dolan in 1987[24]. It is a technique to create patterns on substrate by metal evaporation. Figure 3.1 illustrates the general process of making corral traps, which, consists of three basic steps: mask application, thermal evaporation, and mask removal. Mask application was done by placing 10μm polystyrene beads solution on top of a clean coverslip, letting dry, and depositing 10 nm thin layers of NiCr and AuPd metals. Wherever a bead was located, no metal is deposited on the coverslip due to a masking effect. Beads were then removed from the top of the coverslip by sonication in toluene for 10 minutes. The metal-free, circular holes act as corral traps. This method is relatively inexpensive and commonly used for the production of several different types of metal patterns.

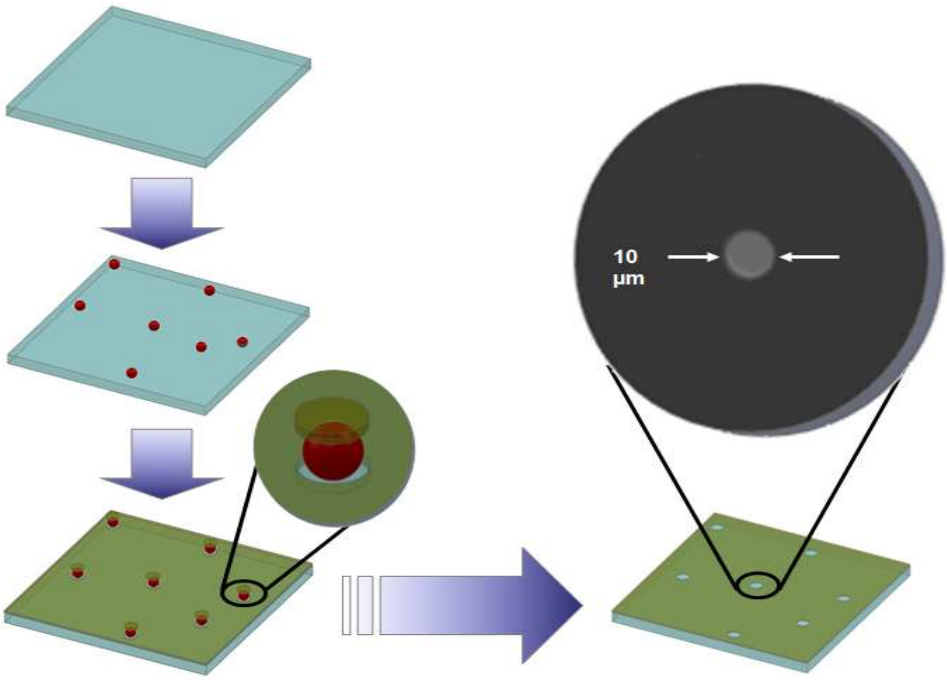

Figure 3.1. Trap fabrication procedure. A dilute solution of 10 μm microspheres is applied to a clean coverslip to serve as a mask. The coverslip and beads are then covered with a thin layer of metal. The mask (beads) is subsequently removed, leaving holes in the metal film. The final image is an optical image of a typical 10 μm hole (40x) [10]. (This figure is taken from Christine Carlson's thesis with her permission).

3.2.1.1 Mask application

The first step of the fabrication is mask application on the coverslip substrate. First, coverslips were cleaned through sonication in an ultrasonic bath for fifteen minute intervals in a series of organic solvents at 35°C:

1) acetone
2) methanol
3) isopropyl alcohol

After sonication, the coverslips are dried under clean nitrogen gas.

In order to create micro-scale traps10 μm polystyrene beads were being used. 1 μL solution of 10 μm polystyrene beads was placed in the center of a

cleaned coverslip, covering approximately 8×10^5 μm^2 of the substrate surface[10]. The coverslip is next allowed to dry at room temperature in a clean environment for 15 minutes.

The 10 µm polystyrene beads stock solution was cleaned and then diluted as following. 2 mL of 10 µm polystyrene beads stock solution from vendor were well mixed in an amber vial and let sit overnight. 800 µL supernatant was removed and 800 µL ultrapure water was added and mixed well. This process was repeated five times. All the micro-scale traps were made using the same processed and cleaned polystyrene beads. Cleaned polystyrene beads were then diluted. A final 1:1000 dilution (25 µg/mL) of the original stock bead solution was produced in ultrapure water[10].

3.2.1.2 Vacuum thermal evaporation of thin metal films

The second step of the fabrication is thermal evaporation. Evaporation is vaporizing material by passing an electrical current through metal on a filament in the evaporator. In a chamber with perfect vacuum, the material evaporates from the source and forms a spherical cloud of vapor that reaches the substrate and deposits metal onto all surfaces. 5 nm thick Nichrome (60:40 Nickel - chromium) were thermally evaporated onto a coverslip with 10 µm polystyrene beads, followed by 5 nm thick Gold-Palladium (60:40). The vacuum chamber had ~4.5×10^{-5}torr pressure, and thermal deposition proceeded at an evaporation rate of roughly 0.1 A/sec[10].Due to lack of thickness monitor the thickness of the metal layer was calculated prior to deposition using equation below:

$$t = \frac{m}{4\pi\rho d^2}$$

where t is the desired film thickness, m is the mass of the metal needed to achieve the desired thickness, ρ is the metal density and d is the distance from the tungsten filament (the source) to the exposed side of the coverslip. After evaporation, the coverslips were investigated under microscope to make sure that they do not have extensive cracks in the thin metal film, which could result in inefficient or lack of electrical conductivity. Cracks after the thermal evaporation is evidence of poor metal film adhesion, and during mask removal, the metal film can crack because of mechanical stress. Reproducibility and reusability of coverslip with traps was difficult due to continuous flaking and cracking of the thin metal film. Other metals were investigated for improvement of the film such as aluminum, silver and gold. Unfortunately, no success was achieved with silver and gold metal due to continuous flaking and cracking of the metal on coverslip. With aluminum metal there was some success, but the surface was oxidized in air making the thin metal coverslip not usable. Nichrome (60:40 Nickel-chromium) is well known for resistance to oxidation and commonly used as an adhesion layer between glass and other metals[25]. Also, it is well known that gold is a good conductor of electricity and does not easily corrode, which is why it is often used in electric connectors[26]. As a result, a layer of 60:40 gold-palladium worked best with adhesion of the nickel-chromium layer.

3.2.1.3 Mask removal

The third step of the fabrication was mask removal. The 10 µm polystyrene beads were removed by sonication of the coverslip in toluene for five to six minutes. Most of the beads were removed during the first attempt, but a few beads were still attached to the coverslip. So, sonication in toluene for five to six minutes was repeated until all the beads were removed from coverslip. Removal of beads was successful with this method, but cracks and tears in the metal film resulting from sonication (mechanical stress) were still sometimes observed on coverslips, especially if sonication of coverslip was done for more than five to ten minutes. To address this problem the time and the cycle of sonication was limited to just two times of five minutes[10]. Then the coverslip was rinsed by isopropyl alcohol and dried with nitrogen gas.

3.2.2 Electrical property of the metal

The metal film on the coverslip provides a conductive layer that allows charges to flow to the embedded traps. An inefficient or lack of electrical conductivity would lead to failure of the experiment; therefore, the electrical conductivity of the metal film was tested on all coverslips. Electrical resistance measurements were taken across thin film with an Ohm meter (Fluke 179, resistance sensitivity ± (0.9%)) in order to determine the resistivity presented in Table 3.1. Resistance is the measure of difficulty electrons have in flowing through a particular object. The resistivity was then calculated by the following equation:

$$R = \rho \frac{l}{A}$$

where R is the resistance of the metal film on the coverslip, ρ is its resistivity, l is the length of the coverslip, and A is the cross section of the metal film.

Table 3.1 Electrical properties of continuous thin metal films that were used as standards.

	Resistance (Ω)	Resistivity (Ω·m)
60-40 Au-Pd	419.49	2.097×10^{-6}
Gold	21.65	1.082×10^{-7}
Aluminum	400.52	2.003×10^{-6}

3.3 Analysis

3.3.1 Digital imaging

Cascade II: 512 (Photometrics, Tucson, AZ) EMCCD (electronmultiplying charged coupled device) camera was used to capture bright-field and fluorescence images of the electrostatic trap. This camera is capable of single photon event detection while maintaining high quantum efficiency (>90%), which is achieved by a solid state electron multiplying register at the end of the normal CCD register and before the A/D converter.

3.3.2 Fluorescence microscopy

A Jablonski diagram (shown in Fig. 3.2) illustrates the fundamental processes that are involved when a photon interacts with a molecular system.

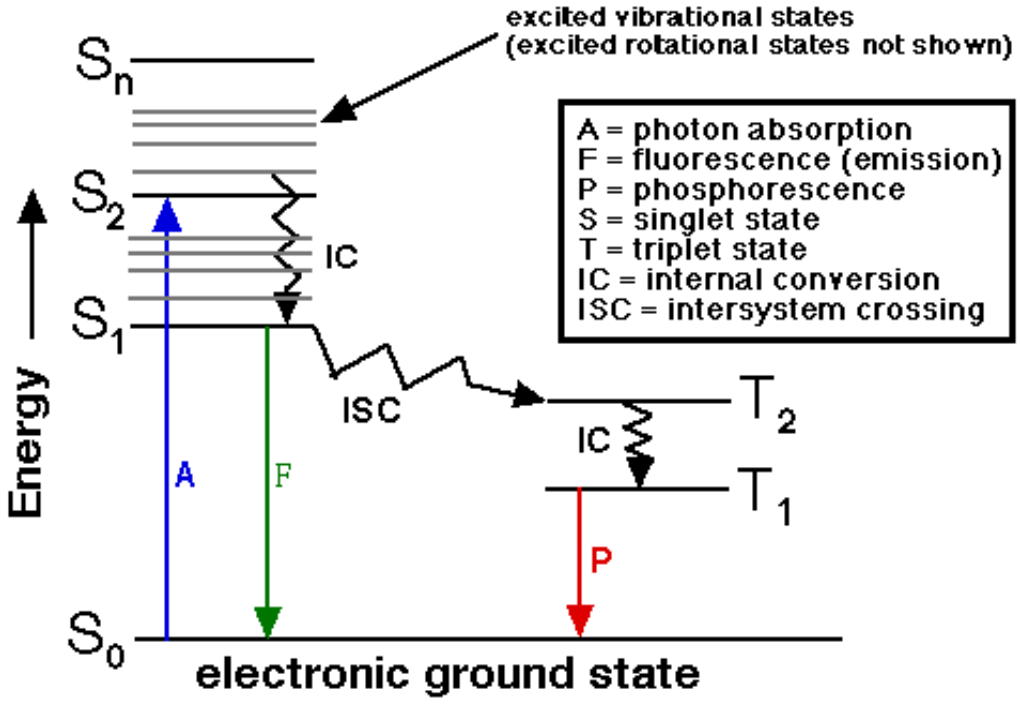

Figure 3.2. The absorption from the electronic ground state S_0 to the different vibrational levels of the corresponding excited electronic level together with the fluorescence and phosphorescence emission are shown. The processes of internal conversion (IC) and intersystem crossing (ISC) are depicted wavy lines indicate fast, radiationless transitions[28].

Fluorescence microscopy is a technique that utilizes fluorescence, the property of some atoms and molecules to absorb a photon of light at a wavelength corresponding to its particular absorption spectrum, and to subsequently emit a photon of longer wavelength or with “red-shifted” energy. (see figure 3.2 for an energy diagram). Since the fluorescence is at a different wavelength than the excitation light (blue arrow in figure 3.2), it can be easily filtered out using high quality optical band pass filters, which block all excitation light and pass only the fluorescence light (green arrow in figure 3.2). In our lab we are using a far- field optical set-up and an argon laser to produce diffraction

limited fluorescence images. The process of phosphorescence (red arrow in figure 3.2) occurs in a manner similar to fluorescence (green arrow in figure 3.2), but with a much longer excited state lifetime because photon emission couples an excited triplet state with the singlet ground state. The fluorescence process is governed by three important events, all of which occur on timescales that are separated by several orders of magnitude. Excitation of a susceptible molecule by an incoming photon happens in femto seconds, while vibrational relaxation of excited state electrons to the lowest vibrational energy level is much slower and can be measured in picoseconds. The final process, emission of a longer wavelength photon and return of the molecule to the ground state, occurs in the relatively long time period of nanoseconds. The “fluorescence microscope” refers to any microscope that uses fluorescence to generate an image, whether it is a more simple set up like an epi-fluorescence microscope, or a more complicated design such as a confocal microscope, which uses optical sectioning to get better resolution of the fluorescent image. All fluorescence microscopy was performed in epi-fluorescence mode by coupling laser light from an argon ion laser (Stabilite 2017, Spectra Physics, Mountain View, CA) into the back port of the Zeiss Axiovert 200M inverted microscope that was also used for bright-field studies. Figure 3.3 shows the setup used for experiments.

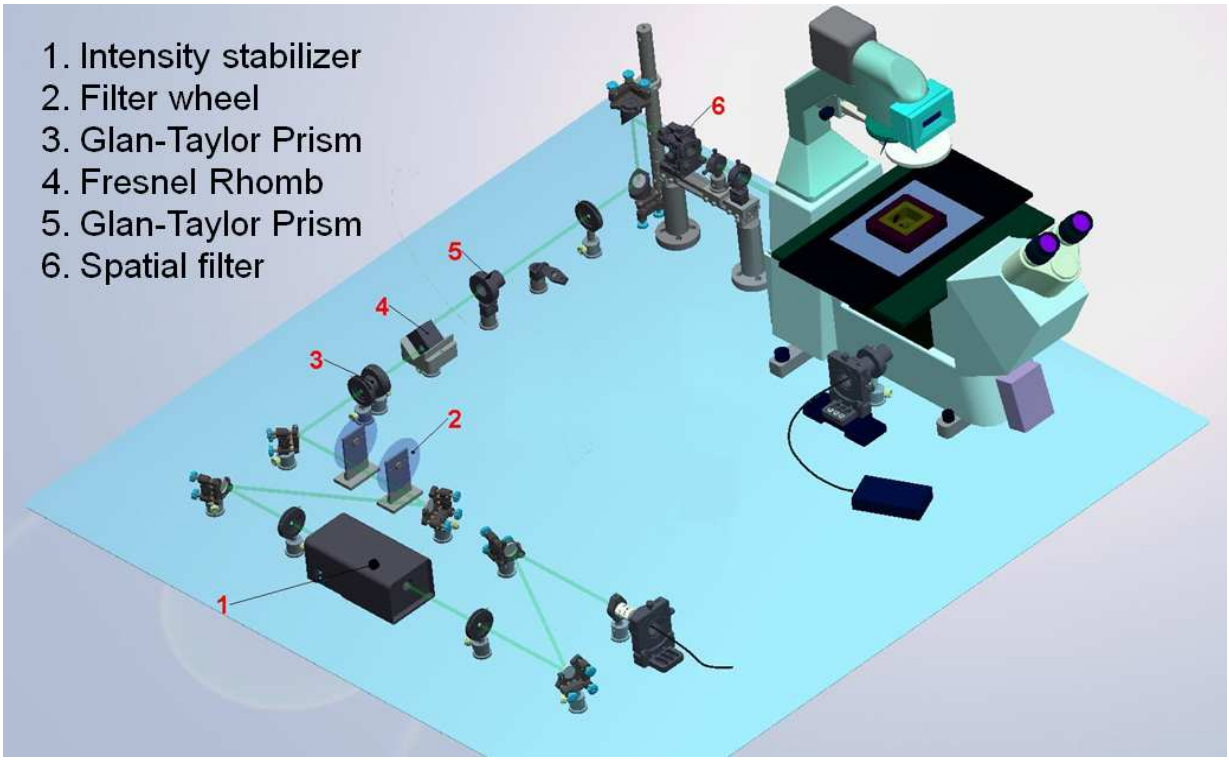

Figure 3.3. Layout of laser light from an argon ion laser into the back port of the Zeiss Axiovert 200M inverted microscope.

3.3.3 Optical microscopy

The optical microscope is a type of microscope which uses visible light and a system of lenses to magnify images of small samples. There are two basic configurations of the conventional optical microscope: the simple microscope and the compound microscope. A simple microscope is a microscope that uses a lens or set of lenses to enlarge an object through angular magnification giving the viewer an erect enlarged image. A compound microscope is a microscope which uses a lens close to the object being viewed to collect light which produces a real image of the object inside the microscope viewed through the eyepiece.

Until the late 1980s, most microscopes had a fixed tube length with a specified distance between the nosepiece opening, where the objective is

attached, and the eyepiece seat in the observation tube[29]. This distance is known as the mechanical tube length of the microscope. When the specimen is placed in focus, it is a few micrometers further away than the front focal plane of the objective (Fig. 3.4a) [29]. Finite tube lengths were standardized at 160 mm during the nineteenth century by the Royal Microscopical Society (RMS), and were in use for over 100 years[29].

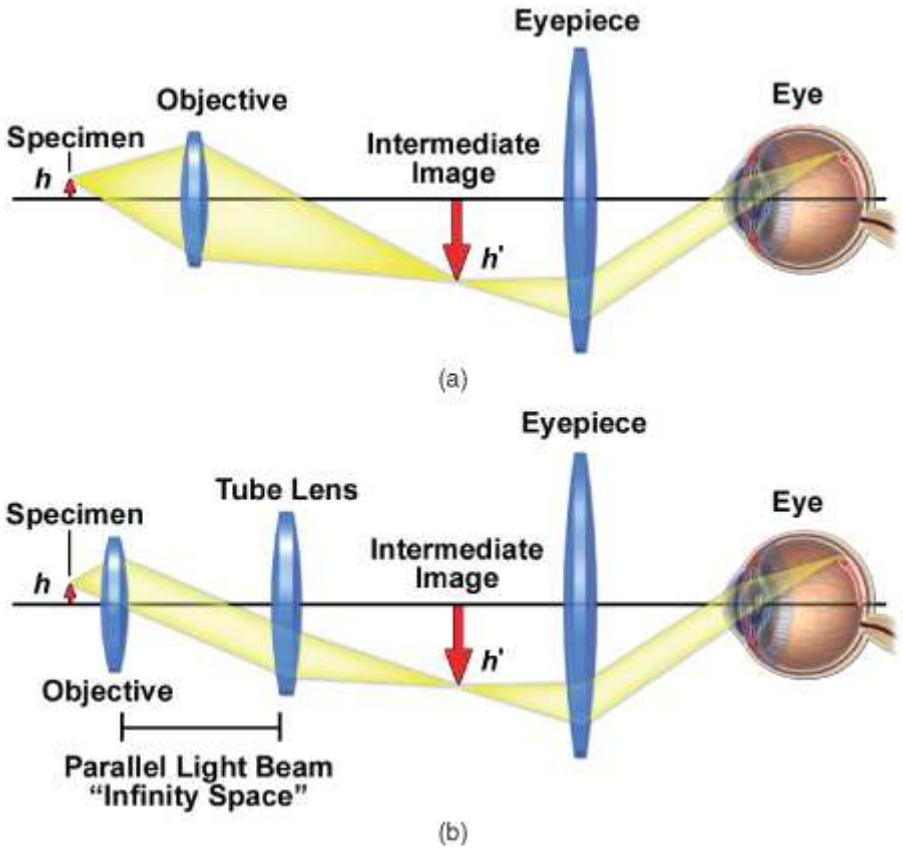

Figure 3.4. Finite and infinity corrected microscope optical configuration. (a) Finite microscope optical train showing focused light rays from the objective at the intermediate image plane. (b) Infinity-corrected microscope with a parallel light beam between the objective and tube lens. This is the region of the optical train that is designed for auxiliary components, such as differential interference contrast (DIC) prisms, polarizers, and filters[29].

Addition of optical accessories into the light path between the microscope frame and observation tube head of a fixed tube length microscope increases the effective tube length to a value greater than 160 mm[29]. Therefore, inserting auxiliary components, such as a reflected light or fluorescence illuminator, polarizers, filters, and differential interference contrast (DIC) prisms, can introduce spherical aberration and host images into a corrected optical system. Infinity optical systems have a different objective design that produces a flux of parallel light wave fronts imaged at infinity, which can then brought into focus at the intermediate image plane by a special optical lens. The region between the objective's rear aperture and the tube lens is called infinity space, as seen in figure 3.4b, where auxiliary components can be introduced into the light path without producing focus optical aberrations (Fig. 3.4b)[29].

Chapter 4

Materials and Experimental Method for Fabrication of a Microfluidic Device

4.1 Overview

Microfluidics opened a new pathway for research and there are virtually unlimited applications of microfluidics in many fields, such as biology, chemistry, biophysics and engineering. With microfluidic devices, a host of information is easily and efficiently obtained with small volumes of fluids, such as, the rapid measurement of diffusion coefficients of large and small molecules in a microfluidic device[30], fluid viscosity[31], determining the *p*H of a multiple samples in separate channels at the same time [32, 33], chemical binding coefficients[30] and enzyme reaction kinetics[34], leading to reduction of reagent used. Quantities of waste produced are also minimized. Microfluidics is used for DNA analysis[36, 37, 38, 39], cell manipulation[40], cell separation[41], flow cytometry[35] and others, leading to dramatic improvements for analysis.

In this chapter materials and experimental methods for fabrication of microfluidic devices will be discussed. This chapter focuses on integrating electrostatic corral traps into a microfluidic device for experiments. Development of microfluidic devices with integrated electrostatic traps is essential for capturing single molecules in their natural environment in order to study their mechanics or dynamics over long time scales. There is room for improvement concerning the setup used so far for trapping molecules; the sample solution dries out typically within 45 minutes, and it is not possible to accurately control the conditions to create a flow that will carry “all” the particles from where they are to where they need to be in order to trapped. Integrating corral trap into microfluidic device will resolve many of these issues. There is one main process used for fabricating microfluidic devices, namely photolithography, that will be discussed in the thesis.

4.2 Instruments

4.2.1 Profilometer to measure thin film thickness

A profilometer is a non-destructive, easy-to-use method of measuring surface high by taking step measurement. The Alpha Step 200 profilometer is used to measure step heights, etch depths, coating thicknesses, micro-roughness and a variety of other high precision surface characteristics. Tencor AlphaStep 200 is used to measure thin film thickness between 10 Å and 165 microns and has resolution 5 nanometers for scan lengths of 80, 400, 2,000, or 10,000 microns. It measures the deflection of a 2D diamond-tipped stylus in direct contact as it is drawn over the sample surface, as shown in figure 4.2. The AlphaStep 200 is equipped with a standard stylus of 12.5 micron radius. Sample leveling is automatically computed after each scan. The scan area is imaged on a, 9-inch CRT. Figure 4.1 shows the instrument used for the thickness measurement. The sample was placed on the black circular surface. A standard from VLSI Standard Inc. 960 Å calibration features was used before every measurement. The standard was off by ±12 Å. The base of the channel was off ±15 Å because of thickness of stylus could not reach the base. The instrument was used in Dr. Carolyn Aita's lab with help of Elizabeth Hoppe.

Figure 4.1. Thin film thickness measurement Tencor Alpha-Step 200 profilometer.

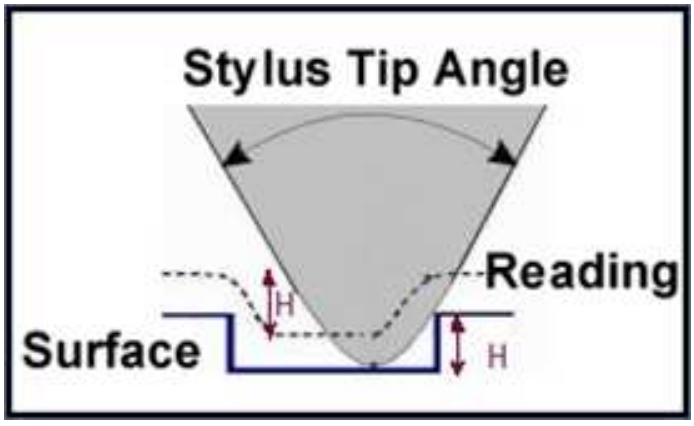

Figure 4.2. Schematic of diamond-tipped stylus in direct contact, as it is drawn over the sample surface.

4.2.2 MJB-3 contact mask aligner

Karl Suss MJB-3 contact mask aligner was used for SU-8 resist processing. It is based in the cleanrooms for high resolution photolithography of the Wisconsin Center for Applied Microelectronics (WCAM) at the University of Wisconsin-Madison, as shown in figure 4.3. This is a standard MJB 3 aligner equipped with a 200 watt mercury short-arc lamp. The filtered light source produces a combination of g-line, h-line and i-line wavelengths between 320-500nm. Optimum line/space resolution is 1.5 microns. The alignment range of the X and Y stage is 6mm and the in plane tilt range is 30°. Alignment is performed manually by manipulating micrometers while observing the wafer and mask under a microscope. A quartz mask is recommended for wavelengths of 320nm while sodium glass masks are adequate for longer wavelengths. The aligner is used during the lithography process, projecting an image onto a wafer that has been coated with a thin layer of photosensitive material called photoresist. Contact or proximity printing is the simplest lithography method. When UV light passes through the patterned area of a chrome mask, it exposes the photoresist on the wafer and a chemical transformation occurs. After developing in a solution bath and rinsing, a pattern is transferred via the remaining photoresist onto the wafer.

Figure 4.3. Standard MJB 3 aligner equipped with a 200 watt mercury short-arc lamp.

4.2.3 Spinner and HMDS

The spinner in figure 4.4 is capable of coating substrates up to 8 inches in diameter. A variety of chuck holders are available at the Wisconsin Center for Applied Microelectronics (WCAM) at the University of Wisconsin-Madison. The spinning speed is adjustable from 500 to 5,000 rpm and an electronic timer automatically controls the spin cycle. For reproducible lithography, the photoresist needs to be uniform and pinhole-free. The standard method of application is spinning. In this method, the substrate is mounted on a vacuum chuck; a metered amount of photoresist is deposited onto the center of the wafer; and then the revolving wafer flings off the excess resist and a uniform film is

produced. The viscosity of the photoresist, rotational speed and time of the spin are the controlling parameters. In figure 4.4, next to the spinner, is shown a chamber for applying the adhesion promoter/primerhexamethyldisilazane(HMDS), which improves the adhesion of the photoresist and provides a contaminant-free resist film.

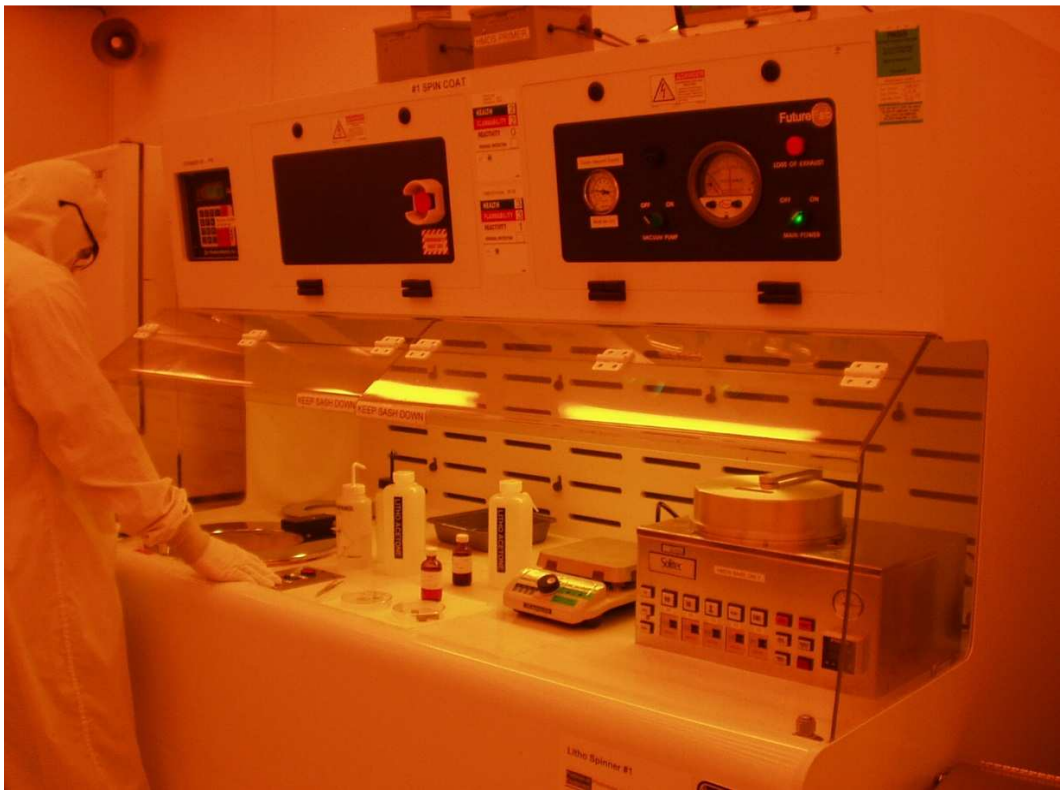

Figure 4.4. Spinner on the left side and HMDS on the right side.

4.2.4 Ion beam sputter coater

This instrument was used in Dr. Carolyn Aita's lab with help of Elizabeth Hoppe. Ion beam sputter deposition is a physical vapor deposition (PVD) method, which (like thermal evaporation) results in a thin layer of conductive metal, such

as gold or palladium, on a substrate surface. The process, however, occurs at higher gas pressures, where ions collide with gas atoms that act as a moderator and move diffusively, reaching the substrates or vacuum chamber wall shown in figure 4.5. The high energy ballistic impact to low energy thermal motion is achieved by changing the gas pressure. The sputtering gas is often an inert gas such as argon.

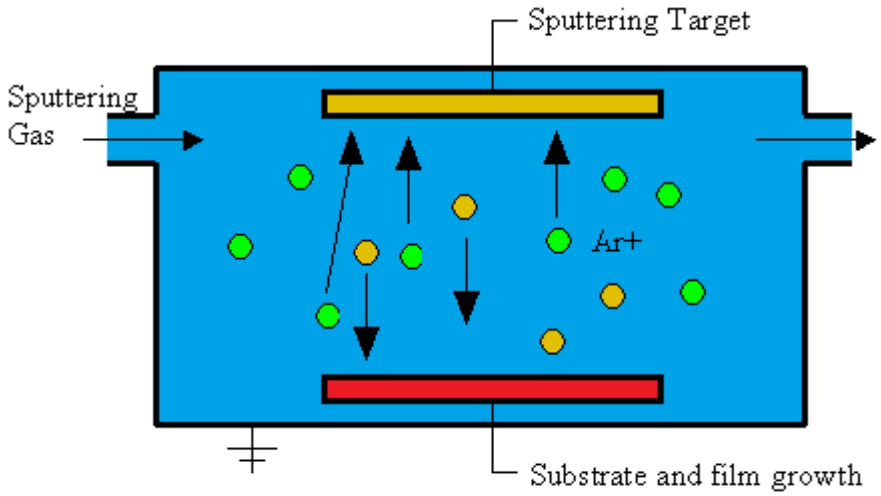

Figure 4.5. Sputter coating process.

4.3 Materials for fabrication of microfluidic devices

Materials in chapter 3 are used as well as following:

- Hexamethyldisilazane (HMDS) (Sigma-Aldrich 999973, grade ≥99%)
- Photoresist s1813, (Shipley)
- 6:1 Buffered Oxide Hydrofluoric Acid (BOE) with OHS (CPG Grade cat # 880406 Fujifilm),
- Developer 321, (Shipley)

- SU-8 (2000.5 series) (Micro Chem, Y1110140500L1GL)
- Sylgard 184 Silicone Elastomer Kit Poly(dimethylsiloxane) (PDMS) (2404019862)

The devices were made by photolithography using two types of photoresist, a positive photoresist where exposure to UV light removes the resist, and a negative photoresist in which exposure to UV light maintains the resist. Figure 4.6 shows a typical positive and negative process of fabrication of microfluidic devices. In a typical process of fabrication photoresist is spin-coated on a substrate, and then a mask with the desired pattern is placed on top of it. The photoresist is illuminated through the mask by UV light, developed using a developer, and the undeveloped photoresist is finally removed by acetone. Both methods for fabricating devices were used and will be presented in detail.

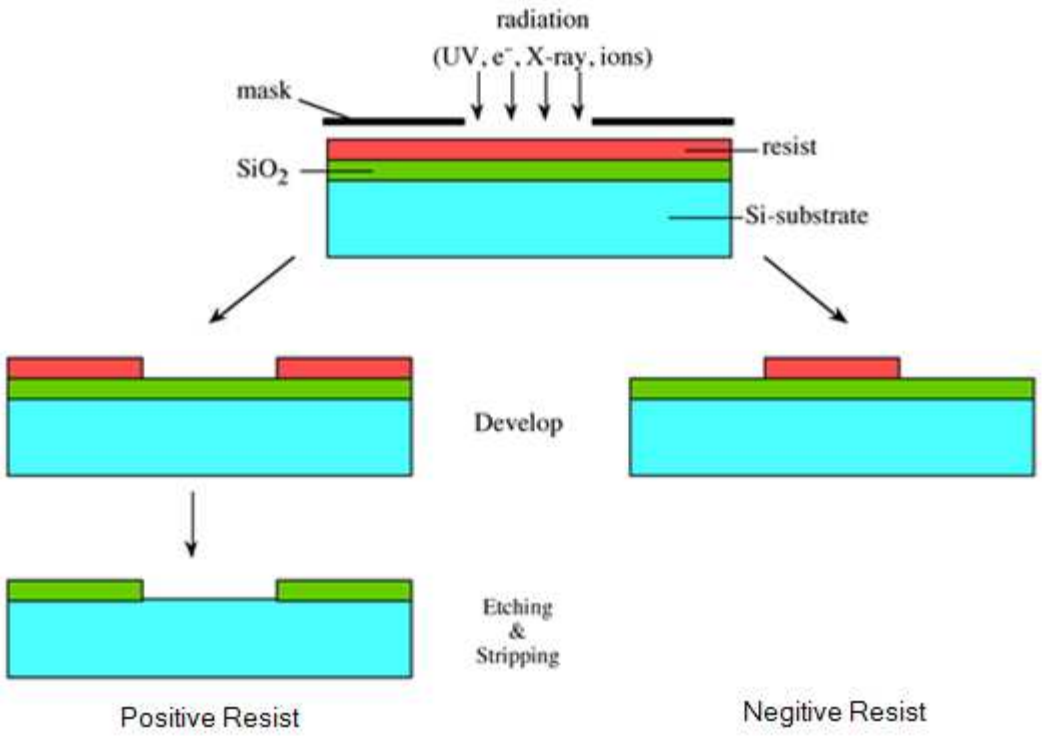

Figure 4.6.Photolithographyprocedure using negative and positive resist.

4.3.1 SU-8 and PDMS photolithography

The purpose of photolithography is to create small structures or features on a silicon wafer using photoresist, and was used to create a mold for the micro-channels. It has some similarities to the process of development of a photograph, except the result is a three dimensional structure. There are three main components in a lithography process: substrate, photoresist, and mask. Figure 4.7 shows the technique for fabricating a microfluidic channel using SU-8 photoresist (negative resist). The result of this procedure is a microfluidic channel, which can hold a stationary solution in the trapping setup. For the experiment the set up consists of a 0.17mm thick glass coverslip with the 10μm traps and 0.5-2 μm thick Poly(dimethylsiloxane) (PDMS) layer with embedded pattern of channel on top of it.

The procedure can be summarized as follows. PDMS base (Sylgard184 Silicone Elastomer Base, Dow Corning Canada) was mixed with Sylgard 184 Silicone Elastomer Curing Agent (Dow Corning Canada) at a ratio of 10:1. The mixture was placed in a vacuum chamber for 30 minutes in order to make it smooth and without bubbles. For this device SU-8 2000.5 was used following the recipe described below. Figure 4.8 shows SU-8 mold made with different designed patterns of channels using this recipe. SU-8 molding was done in Dr. Woo-Jin Chang's lab at University of Wisconsin-Milwaukee using the recipe described below.

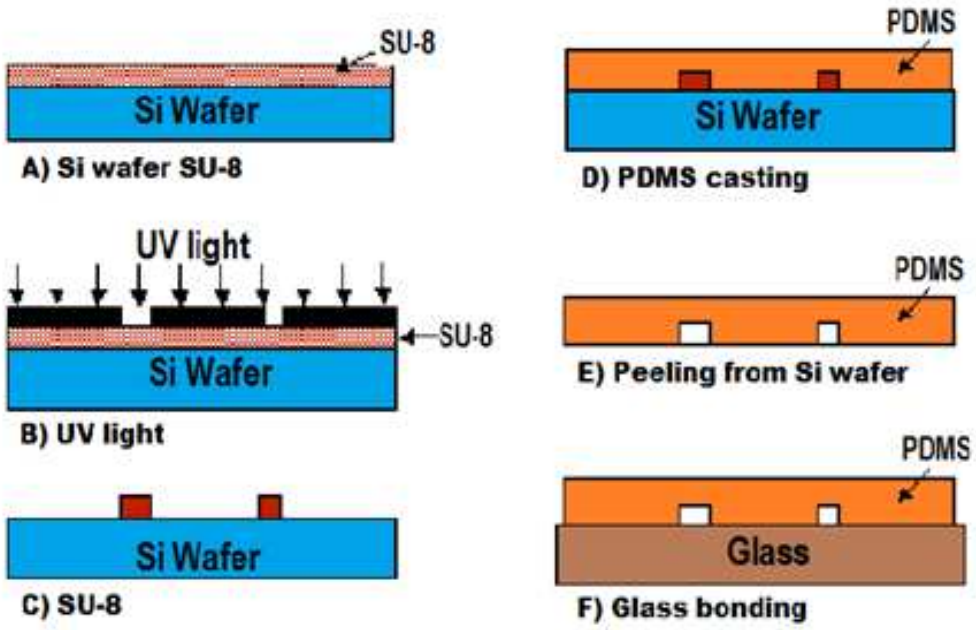

Figure 4.7. Lithography using SU-8 (2000.5) and PDMS.

The recipe to build the device is as following:

1) Substrate pre-treatment
    a. Soak in sulfuric acid, hydrogen peroxide
    b. Heat at 15°C for 10 minutes
    c. Wash with acetone, isopropyl alcohol and water repeatedly
    d. Air dry with N_2 gas
    e. Put wafer on hot plate for 5 minutes to remove any water
    f. Spray with N_2 gas
2) Coat
    a. Pour 1mL of SU-8 2000.5 per 1 inch of wafer diameter.
    b. Spin at 500 rpm for 5 minutes with an acceleration of 100 rpm/second
    c. Spin at 3000 rpm for 30 seconds with an acceleration of 300 rpm/second

d. This will result thickness of less than 0.5 μm of SU-8 2000.5.

3) Edge bead removal

   a. Remove buildup of SU-8 2000.5 on edges of wafer to enable close contact with photomask.

4) Soft Bake

   a. Bake SU-8 2000.5 at 95°C for 1 minute.

5) Expose

   a. Put wafer with SU-8 2000.5 in an aligner for UV exposure at 60 mJ/cm^2.

6) Post exposure bake

   a. Bake SU-8 2000.5 at 95°C for 1 minute.

7) Develop

   a. Submerge SU-8 2000.5 in developer for 1 minute

8) Rinse and dry

   a. Spray and wash SU-8 2000.5 with isopropyl alcohol for 10 minutes.

   b. Air dry with N_2 gas.

9) Hard bake

   a. Bake SU-8 2000.5 at 150°C for 5 minutes.

10) Soft lithography (PDMS process)

   a. Mix curing agent:base in 1:10 ratio by mass and mix it well.

   b. Pour the mixture on the SU-8 mold and let it sit in air to remove all the bubbles.

   c. Then bake for 5-6 hours until PDMS gets hard.

d. Remove PDMS from SU-8 mold and attach on coverslip with the micro-scale traps.

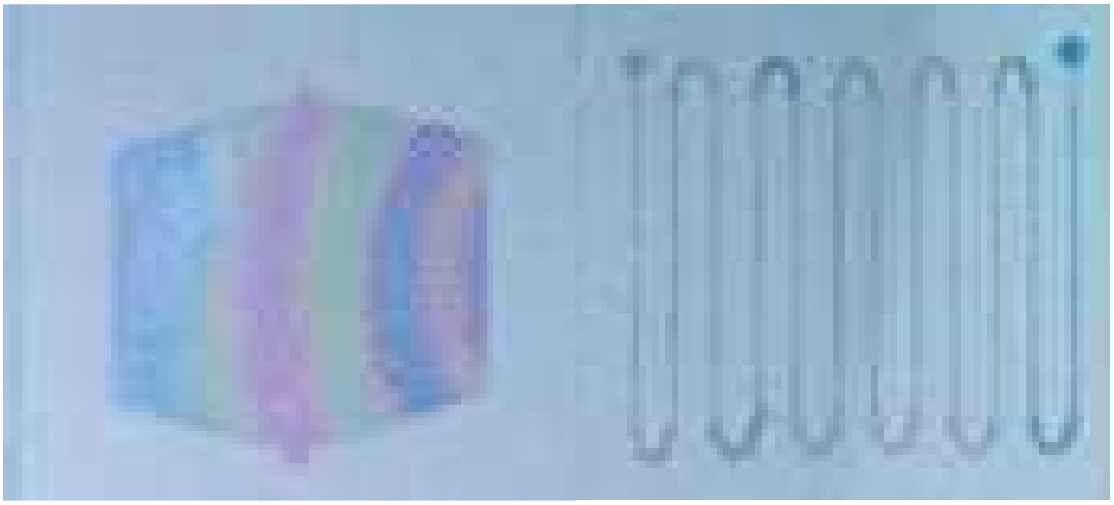

A) B)

Figure 4.8 a, b. SU-8 mold with different channel patterns.

Figure 4.8 a, b shows a mold made with SU-8 photoresist. Figure 4.8a shows a channel supported by lots of poles (circular dots in figure 4.8a), that prevent the large channel from collapsing due to PDMS being very flexible. PDMS process is called soft lithography. The most challenging part of soft lithography is keeping the channel from collapsing. Figure 4.8b shows a continuous channel from right to left without poles using SU-8 photoresist mold. Figure 4.9 shows thin film thickness measurements done with the Tencor Alpha-Step 200 profilometer of a channel pattern in SU-8 mold. Many channels were measured and yielding an average SU-8 mold thickness of approximately 260 nm, which was close to the desired channel depth. In the profile the side lines are not straight and the top is not flat, because the mask used was produced in house on transparency film using a laser printer; therefore, the quality of the

mask was poor. Due to poor quality mask the side walls of SU-8 do not show sharp edges in figure 4.9.

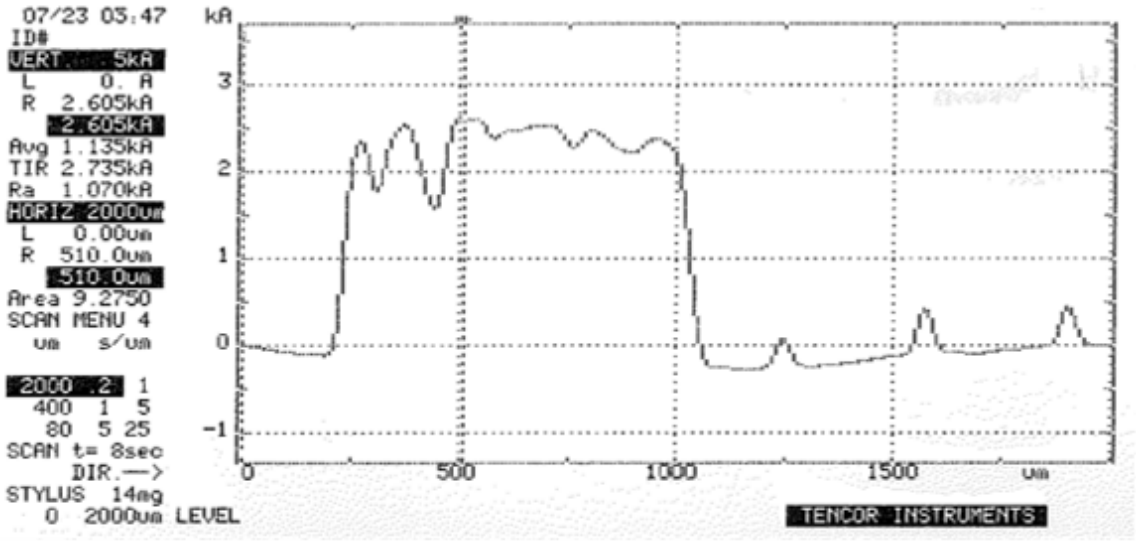

Figure 4.9. Profile of channel made by SU-8 mold in figure 4.8b is approximately 260nm (analysis done with help of Elizabeth Hoppe).

The last part is bonding PDMS to the metal surface. Here the thin metal film with micro-scale traps on coverslip (bottom) is bonded to PDMS (top). Bonding PDMS to non-glass surface is done by plasma bonding. For our device the PDMS adheres to the metal well without plasma bonding, but it can be peeled off. The devices are a little more delicate because of this.

4.3.2 Photolithography etching process

Photolithography using a positive resist to etch channel was our preferred process of making channel. This process is similar to the above mentioned process, but with slight modifications. Figure 4.10 shows the technique for fabricating a microfluidic channel using photoresist s1813 (positive resist). The result of this procedure is a microfluidic channel, which can hold a stationary solution in the trapping setup. For the experiment, 0.17 mm thick 18 mm x 18 mm

coverslip with etched channel and with two holes for inlet and outlet of fluid was made using s1813 photoresist . Sharp edges and flat channels cannot be accomplished using regular glass coverslips (not quartz) due to impurities in the glass. Therefore, use of a pure silica (quartz) coverslip is essential in order to achieve well define channel. Figure 4.10 shows the process of channel made by HF etching using s1813 photoresist.

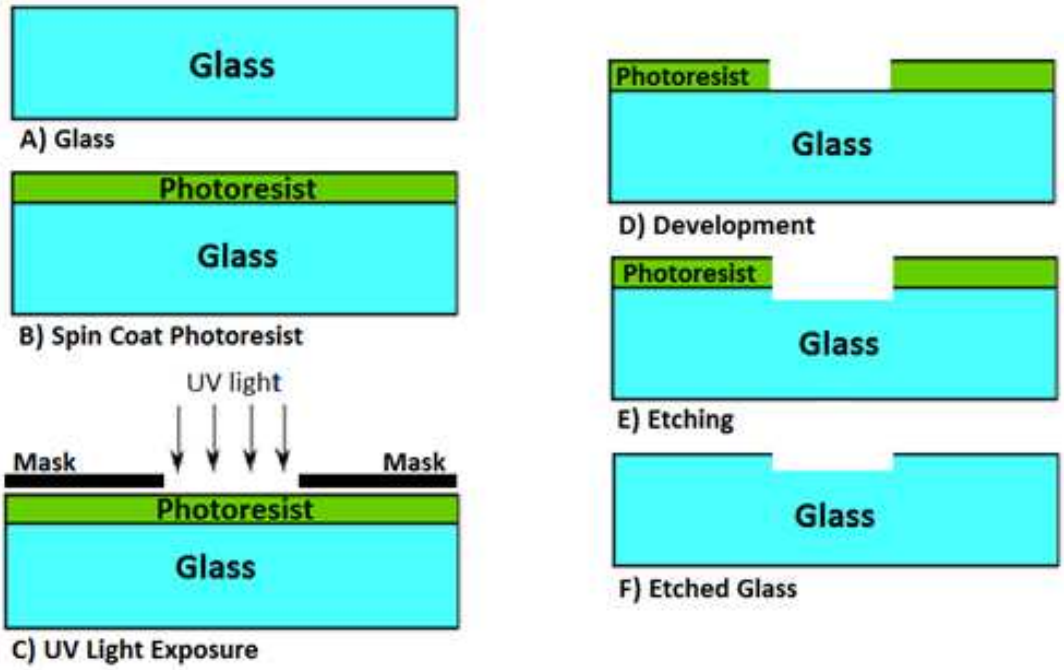

Figure 4.10. Photolithography HF acid etching process.

The receipt used to make channels is as following:

1) 19 mm by 19 mm quartz coverslip is cleaned at 35°C for 15 minutes with
    - Acetone
    - methanol
    - Isopropyl alcohol
    - Dried with N_2 gas

2) The quartz coverslip is placed in vaporized HMDS chamber with vacuum at 105°C.
3) Spin coat photoresist s1813
    - Spin coat as follows:
    - Step 1: 10 seconds, 500 RPM, 500 Ramp
    - Step 2: 30 seconds, 4000 RPM, 1000 Ramp
    - Step 3: 0 second, 0 RPM, 500 Ramp
4) Put quartz coverslip with photoresist on a hot plate for 1minute at 115°C.
5) Take the quartz coverslip with photoresist to MJB-3 contact aligner with the mask.
6) Line up the mask and coverslip on the instrument and set up exposure time to 18 seconds.
7) After exposure to UV light, take the quartz coverslip to develop.
8) Use base 321 to wash PR s1813 for exactly 45 seconds.
9) Dip the quartz coverslip under running water for 10-15 seconds.
10) Dry quartz coverslip with air.
11) Take the quartz coverslip for etching with Hydrogen Fluoride acid (HF) buffered oxide etch 6:1(BOE) for exactly 10 minutes.
12) Then put quartz coverslip in running water for 5 minutes.

Figure 4.11 shows coverslip with the channel made by above recipe and the channel's shape with the two circles at the end of the channel. Figure 4.12 shows profile done on the same coverslip across the channel to determined the depth of the channel. From 10 minutes etching, the channel depth came out to be

870 nm using a Tencor Alpha-Step 200 profilometer, very close to the intended depth of 1μm. A 960 Å standard from VLSI Standard Inc. was used before every measurement. The standard was off by ±12 Å. The base of the channel was off ±15 Å of the level due to thickness of the stylus. The side of the channel (under-etching) is a problem as the etchant enters into the substrate, resulting in non-vertical edges; however making microfluidic channels with the HF acid etching process produced the best results with quartz coverslips. However, in contrast to the glass coverslips, we could no longer etch inlet/outlet holes into quartz coverslips with HF acid.

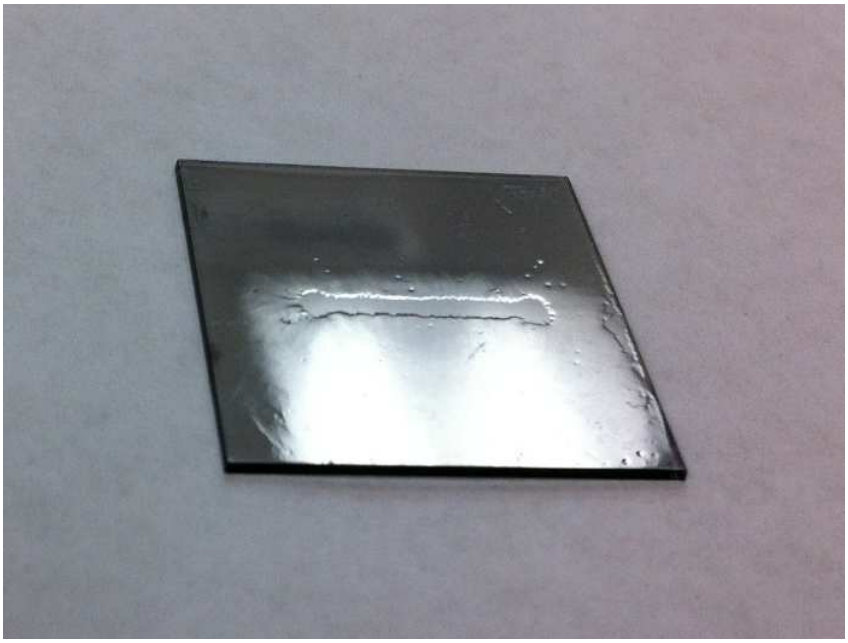

Figure 4.11. Channel made by photolithography HF etching process, the coverslip has a thin layer metal deposited so that the channel is better visible.

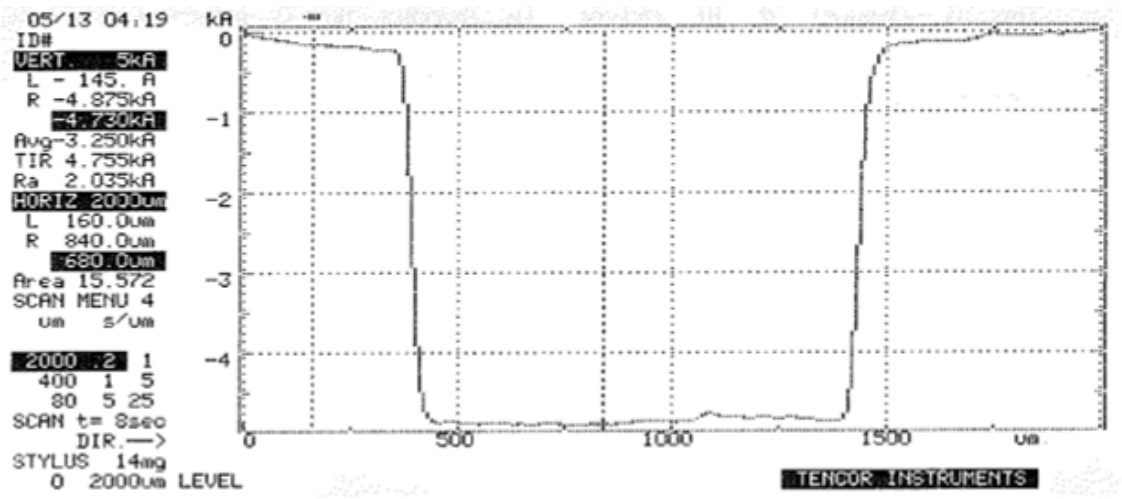

Figure 4.12. Profile of channel of approximately 870 nm made by HF etching. (analysis done by help of Elizabeth Hoppe).

Making two holes on the coverslip for inlet and outlet for the fluid, has been achieved by HF acid etching through the 0.17 mm thick glass coverslip. This was done by attaching two hollow Teflon tubes to the coverslip by UV glue around the tubes, but not inside the holes of tube (shown in figure 4.13a). The tube was then filled with HF (49%) acid and left there for two hours until the HF acid etched all the way through the coverslip (results shown in figure 4.15). The holes can only be made on regular glass coverslip with thickness of 0.17 mm. However, quartz with thickness of 0.5 mm failed to produce holes using this procedure. Therefore, the quartz coverslip was covered with beeswax (except for the locations of the desired inlet/outlet) and dipped in HF acid for 12-15 hours. The holes were made, but the coverslip formed an uneven surface as seen in figure 4.16. Because the holes on the coverslip were made prior to etching the channel; the channel could not be etched with sharp edges. Other methods were devised to make holes in quartz coverslips such as, sand blasting (which breaks

the coverslips), diamond bit drilling (which also breaks coverslips), ultra sonic drilling (didn't make holes at all) and by covering coverslip by photoresist then etching with HF acid (the photoresist came off after 2-3 hours in the HF acid).

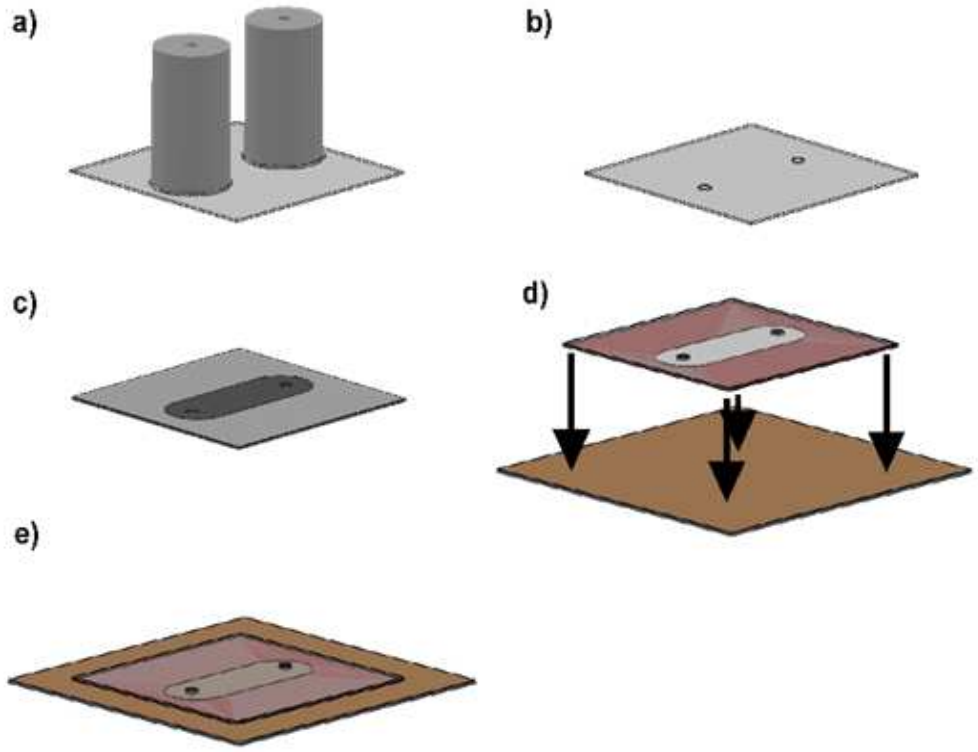

Figure 4.13. a) Teflon tubes define the location of holes for outlet and inlet on the 18 mm x 18 mm coverslip, fabricated by filling the tube channels with HF. b) Coverslip (18 mm x 18 mm) with two holes after Teflon tubes are removed. C) Coverslip (18 mm x 18 mm) with the mask on top. d) Coverslip (18 mm x 18 mm) on top of coverslip (25 mm x 25 mm) with corral traps in a thin metal film. e) The final fluidic device.

Figure 4.13 shows how all the components were assembled together to produce a microfluidic device. Figure 4.13a shows Teflon tubes attached to coverslip to make holes after two hours of HF acid etching like figure 4.13b. Then channel was etched using a photolithography process and HF acid etching as

shown in figure 4.13c. Then ,using 3-trimethoxysilypropylmercaptan, the coverslip with 10µm corral traps is attached to the quartz coverslip with the channel, as shown in figure 4.13d. The attachment of two coverslips cannot be achieved for quartz. Figure 4.14 shows how a coverslip (SiO_2) is attached to coverslip with AuPd metal by 3-trimethoxysilypropylmercaptan ($C_6H_{16}O_3SSi$). The OH groups are present on the channel coverslip surface and AuPd is present on opposing corral trap coverslip. 3-trimethoxysilypropylmercaptan is added to the corral trap coverslip and sandwiched together with channel coverslip. Then, the sandwiched coverslips are left overnight for curing. During the curing process, one bond from each silicon of 3-trimethoxysilypropylmercaptan is covalently linked to the oxygen on substrate surface, as shown in figure 4.14. Each thiol is linked to gold on the surface of subtract providing a monolayer coverage throughout the whole coverslip.

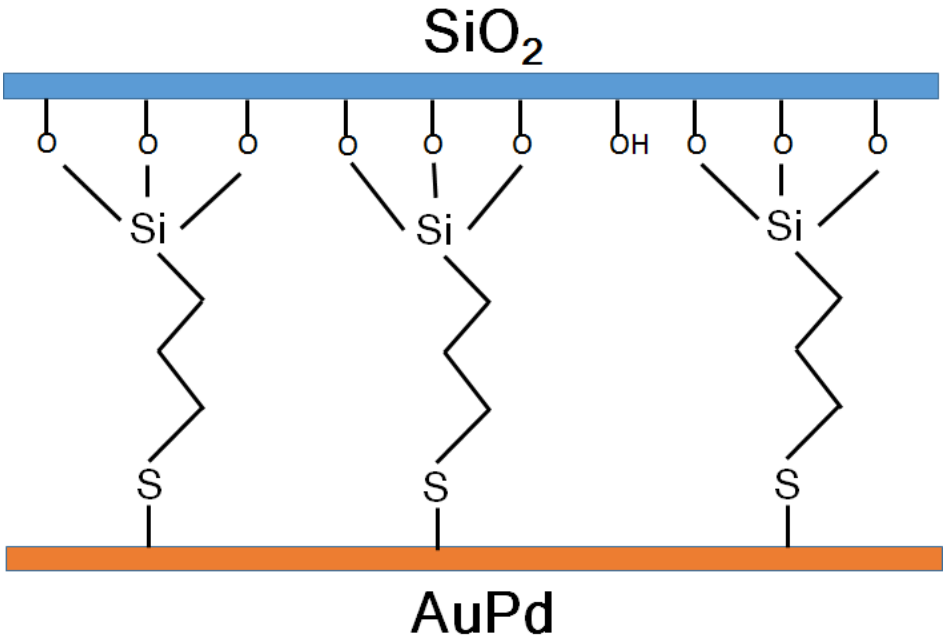

Figure 4.14. Two coverslips are linked together by 3-trimethoxysilypropylmercaptan.

Figure 4.13e shows the final assembled device. A tube with a syringe is attached to the inlet hole, while a tube connected to a beaker collects fluid at the outlet hole. As stated before, the biggest challenge in making this device is making holes for inlet and outlet for fluid on both glass and quartz coverslip.

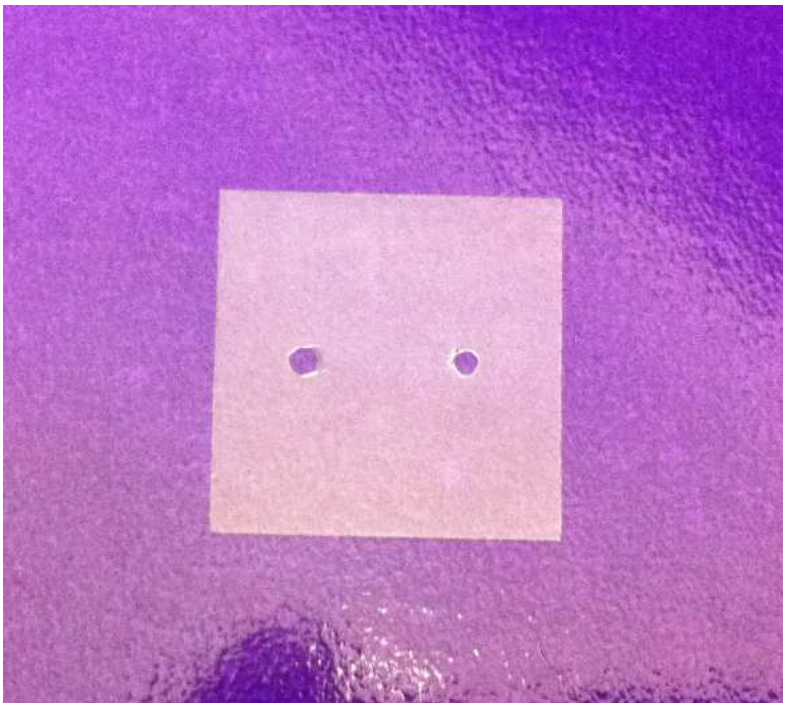

Figure 4.15. Hole made on a glass coverslip by HF acid etching.

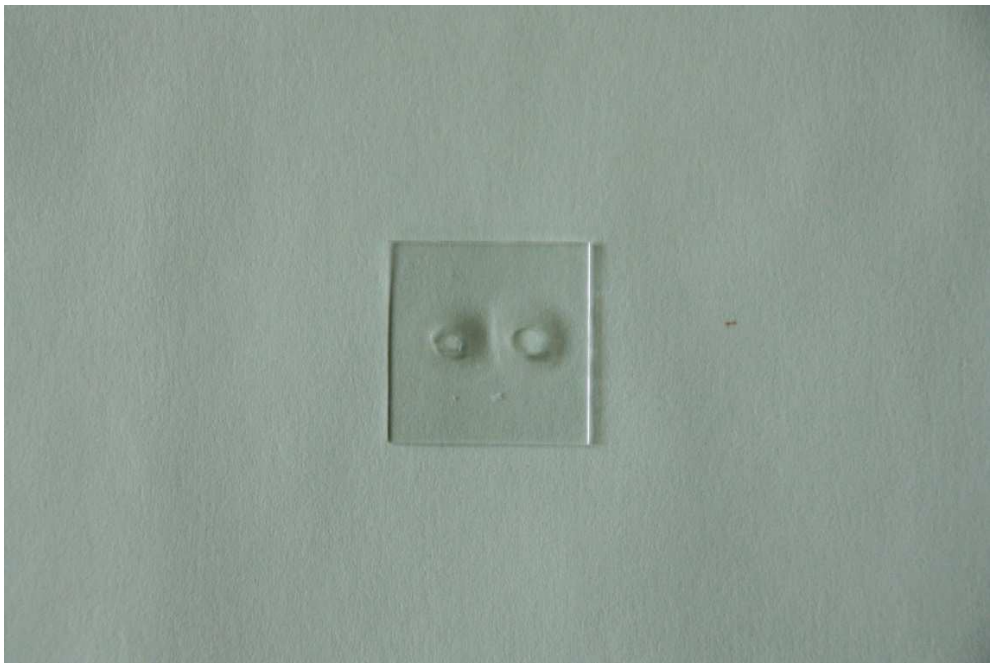

Figure 4.16. Holes made by covering quartz coverslip with beeswax and placing in HF acid.

4.3.3 Other methods for fabricating a microfluidic channel

Many methods for fabricating microfluidic channels were experimented with. One of them is shown in figure 4.17, were aluminum was evaporated on 18 mm x 18 mm coverslip to make the sidewalls of the channel. Unfortunately, we were unable to deposit a thick enough layer due to instrument limitations. Aluminum was approximately 50 nm thick (this is estimated based on material used due to the lack of a thickness monitor in the evaporator). The desired channel depth was at least 500 nm; therefore this was not used for fabricating channels.

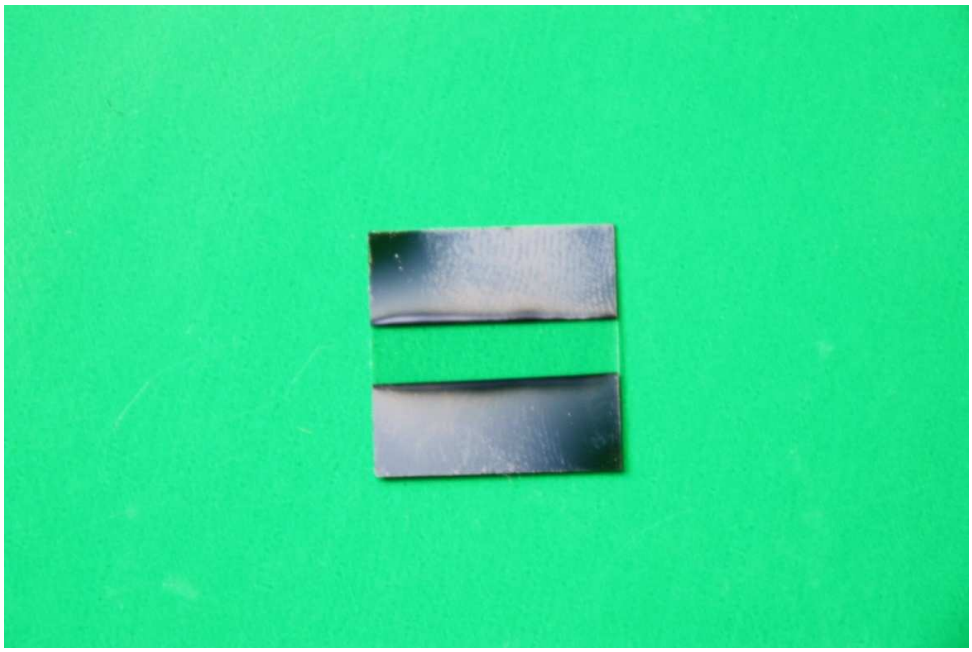

Figure 4.17. Thermal evaporation of Aluminum metal on 18 mm x 18 mm coverslip.

The second method tried to make channels was using sputter coater to deposit the channel walls. Figure 4.18 shows HfO_2 deposition on a 18 mm x 18 mm coverslip with different patterns on coverslip. The maximum thickness we achieved by sputter coating HfO_2 was 280 nm, while the desired thickness was 1000 nm. Also, Hafnium (Hf) was sputter coated as well and the measured thickness was only 250 nm. The thickness measurements were carried out using Alpha-Step 200 profilometer, and the instrument was calibrated using a standard every time.

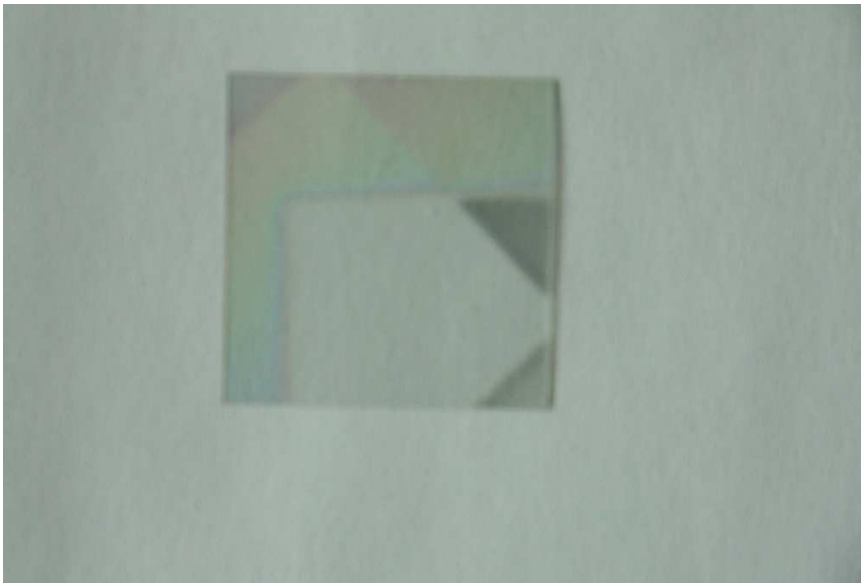

Figure 4.18. Sputter coating of HfO_2 with the pattern seen on coverslip (analysis done by help of Elizabeth Hoppe).

4.4 Displacement rate

We have built many devices to control solution flow inside a confine space, because the direction of the flow as well as control of the displacement rate is essential for experiments. Fluids confined in these structures exhibit physical behaviors not observed in larger structures. In many microfluidic devices, syringe pumps are used to control liquid flow. However, even at the lowest speed these pumps produce particle displacements in shallow channels that are too rapid for corral trapping. In our microfluidic device, we therefore use gravity induced convective flow. Gravity induced flow is achieved by adding two drops of solution on top of each holes, one drop smaller than the other as shown in figure 4.19. It is well known in microfluidics that the flow of the solution is controlled by the volume of the drop, the surface free energy of the liquid, or the resistance of the microchanne[43]. The flow is induced in the direction of the bigger drop as shown in

figure 4.19, due to the surface tension in a drop of liquid[43], channel resistances[43] and the PDMS material being hydrophobic. Other materials can be used, but the drop gets spread on the surface, which lowers the pressure inside the channel.

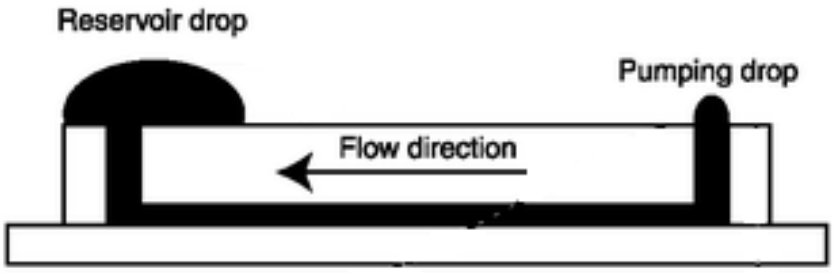

Figure 4.19. Side view of a microchannel. A reservoir port with a large drop and pumping port with a smaller drop are required for fluid flow[43].

Figure 4.20 shows sequence of images with red arrow pointing at a 20 nm bead that was used to calculate displacement rate of the solution in the microfluidic device. In our device flow of the particle varies from the beginning of experiments to after 20 minutes in to the experiments because of evaporation of the solution drops on the surface of the holes. Approximately 9 μm/s displacement rate has been calculated from the single 20nm bead traveling in figure 4.20. Such a flow rate is still about an order of magnitude higher than the desired rate for corral trapping, but can be further adjusted by fine-tuning inlet and outlet hole size and the viscosity of the solution.

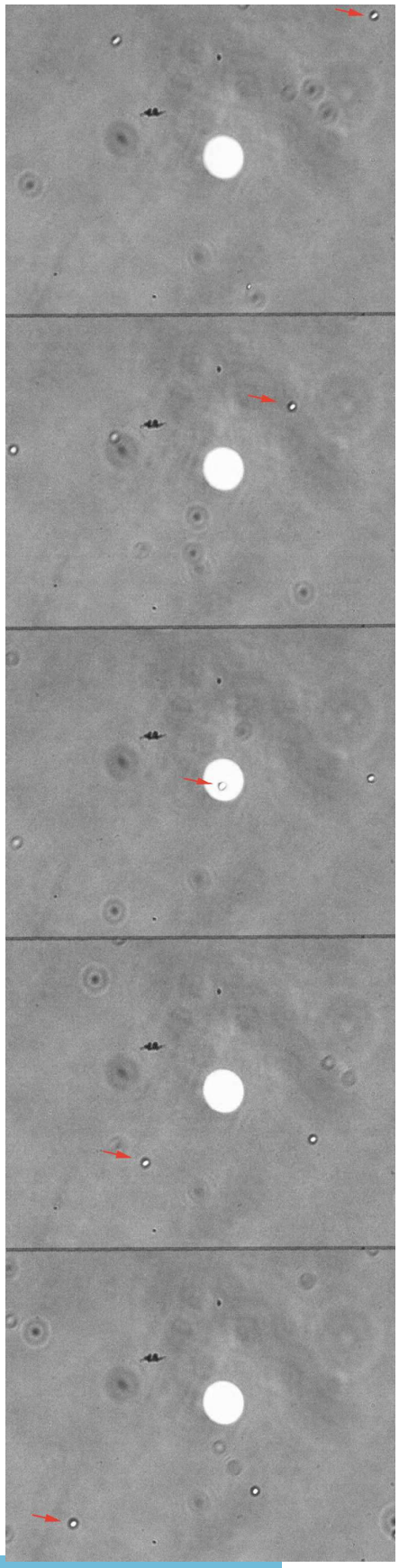

Figure 4.20. The sequence of images where red arrow shows a 20 nm bead traveling in a solution has been used to calculate displacement rate of a bead traveling in microfluidic device.

Chapter 5

Trapping Experiment

5.1 Overview

The theory of corral trapping was presented in Chapter 1. This method has advantages of size, and depends only on particle charge. In this chapter the instruments used for the analysis of trapping experiments, as well as sample preparation and experimental setup are presented. Trapping of polystyrene bead and ssDNA results are described.

5.2 Instruments and analysis

5.2.1 CCD camera

Our main source device for acquiring the images and videos, is a high performance CCD camera (charge coupled device). In a CCD video camera, light hitting the image sensor is converted to an electrical signal. This electron packet must then be transferred one pixel at a time through an output node to an image processor, at which point it is converted into a digital signal by the analog-to-digital converter (ADC) that is then sent to the computer. All the data being collected is being processed by Matlab.

5.2.2 Matlab

Mathworks Inc. specializes in mathematical computing software called Matlab. Matlab can be used for range of applications, including signal processing and communications, image and video processing, control systems, test and measurement, computational finance, and computational biology. Here we use it for image and video processing by writing specific code to carry out the experiment and analyze experimental data.

5.3 Trapping polystyrene bead

In the experiment 20 nm spherical charged polystyrene microspheres beads were used. The experiment was conducted using the fluorescence signal since these objects are small and hard to image under brightfield conditions. Images of the sample were acquired at 1s intervals with an exposure time of 100 ms.

5.3.1 Sample preparation for beads

For the experiment the sample consisted of a 2×10^{-6} g/L stock solution of 20nm polystyrene spheres (Invitrogen F-8827) in a solution of 1.0 mol L^{-1} sodium hydroxide which was titrated to *p*H 10 in order to fully deprotonate the carboxylic acids on the microsphere surface. This solution was freshly made before use.

5.3.2 Experimental setup

A trap was found on the trapping electrode which had been created through the shadow evaporation method using a ~5 nm thick layer of 60:40 NiCr followed by AuPd on 25 mm x 25 mm coverslips. Contact was made to the thin metal film through the attachment of a thin copper wire by a carbon tape as shown in figure 5.1. A 1 µL drop of the 20 nm microsphere solution was deposited onto the trapping electrode in the region of a corral trap, then a second non-metalized 18 mm x 18 mm ozone-cleaned coverslip was placed over the sample, and slight pressure was applied to spread the microsphere solution as much as possible while maintaining a continuous fluid film.

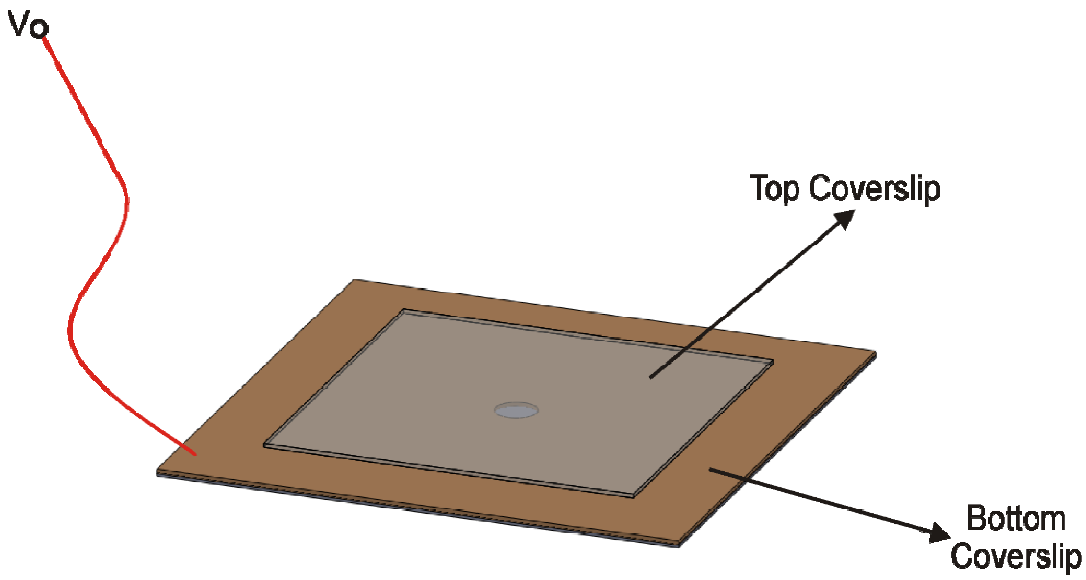

Figure 5.1. Set up of experiment where 25 mm x 25 mm coverslip with corral traps with (attached to a thin copper wire) on the bottom and 18 mm x 18 mm plain coverslip on top with solution in between.

A successful trapping experiment is shown in Fig. 5.2.The sequence of images clearly shows that the microsphere is successfully held inside the trap for the duration of the applied potential, and is released as soon as the voltage is turned off. However, trapping is not always observed with other sample preparations, probably due to a wide variation of the actual charge load on the individual beads. Electrophoresis tests also indicated that only some beads were charged, while others did not seem to be charged at all.

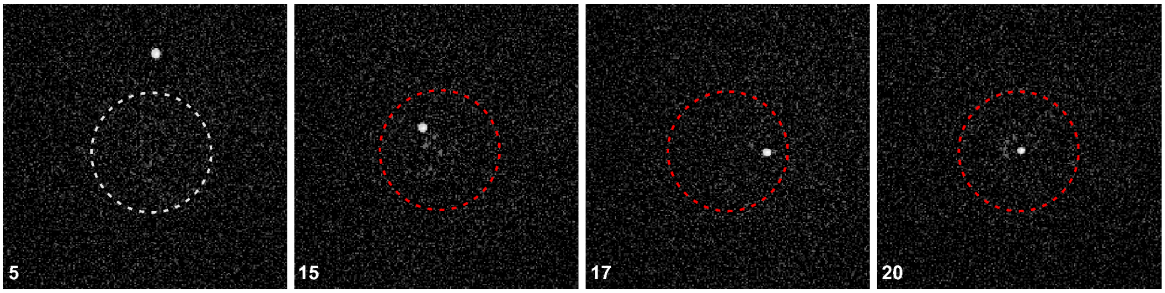

Figure 5.2. Zooms of four frames, of a longer video sequence of a -30 V trapping event of a negatively charged, 20 nm nanobead inside a 10 μm electrostatic corral trap. The circle (red if trap is active) outlines the location of the corral trap, as determined from a brightfield image of the same area. (This figure is taken from Christine Carlson's thesis with her permission[10]).

5.4 Trapping DNA

Corral trap has shown to trap negatively charged particle in the center of the trapping area by applying negative trapping potentials. In subsequent experiments 600-nucleotide single stranded DNA molecules were used. The ssDNA carries a negative charge due to deprotonated phosphate groups on the phosphodiester backbone (seen in figure 5.2). Each ssDNA molecule was covalently linked to a single Cy3 fluorophore, whose chemical structure is shown in figure 5.4. Cy3 belongs to the group of cyanine dyes. The word cyanine is from the English word cyan, which conventionally means a shade of blue-green. Cyanine dyes have many uses as fluorescent dyes, particularly in biomedical imaging. The ssDNA molecule was imaged by fluorescence excitation of the Cy3 dye. Figure 5.5 shows excitation and emission spectrum of Cy3-ssDNA in pH 7.2 buffer[44].Cy3 conjugates can be excited maximally at 550 nm, with peak emission at 570 nm and can be excited to ~ 50% of maximum with an argon ion laser[44].

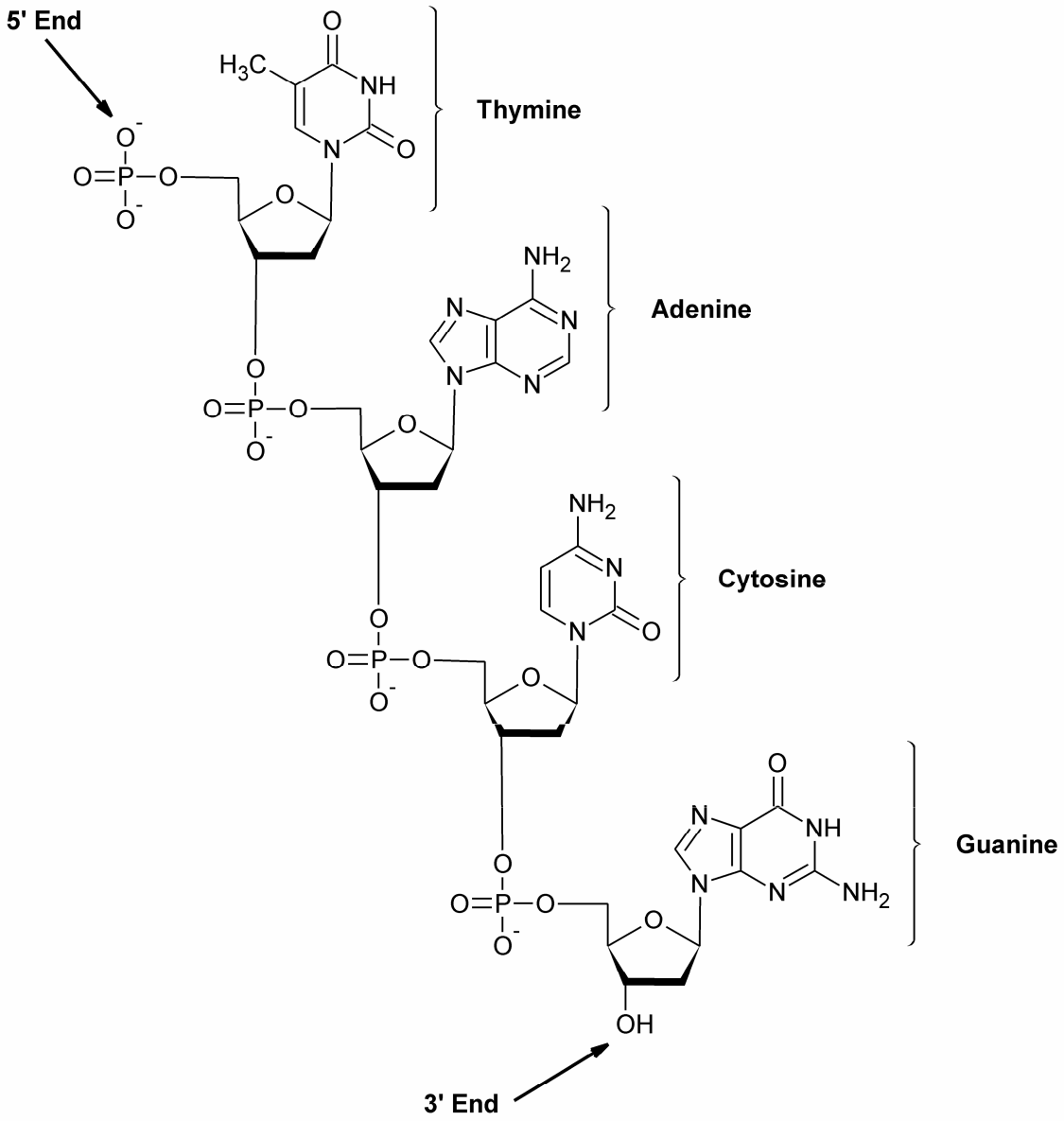

Figure 5.3. Chemical structure of a single strand DNA.

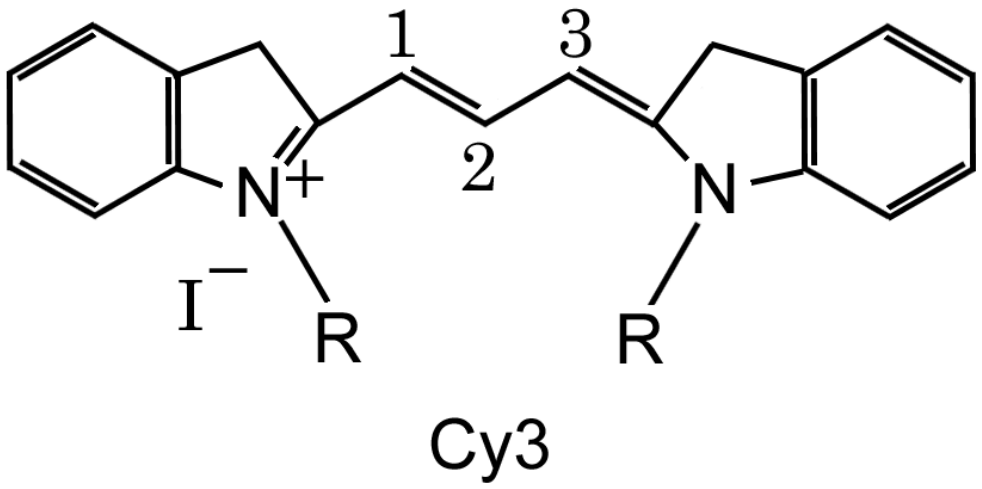

Figure 5.4.Chemical structure of a Cy3.

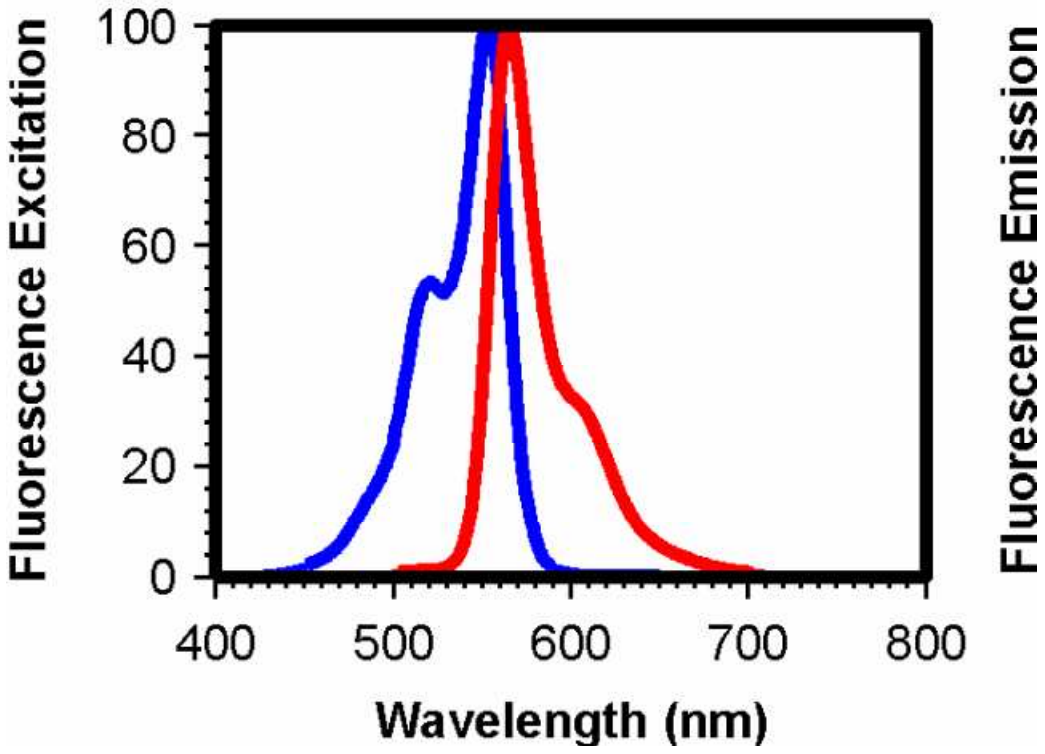

Figure 5.5.Excitation and emission spectrum of Cy3-ssDNA (550/570) in pH 7.2 buffer[44].

5.4.1 Experimental setup

The experiment was conducted under fluorescence imaging conditions, which allows for the observation of the molecules fluorescence signal, since these molecules are too small to be seen in a conventional microscope. The emitted light was collected by a 100× oil immersion objective (α-Plan-FLUAR 100X/1.45; numerical aperture: 1.45, Carl Zeiss Inc.) and imaged with the EMCCD camera. The sample was illuminated by the 514.5 nm line of an argon Ion laser (Stabilite 2017-AR,Spectra-Physics). The laser light was coupled into the back port of the inverted microscope and focused near the back focal point of the microscope objective(epifluorescence mode). In this case, a set of optical filters adapted to the laser line and the fluorescence emission characteristics of the investigated sample were employed (excitation filter z514/10, dichroic filter z514rdc, emission filter hhq519lp; Chroma Technology). Images of the sample were acquired using the multiplication gain amplifier at 5 MHz readout rate with an exposure time of 100 ms, a frame rate of 7.6 fps. The data of the experiment was acquired with the CCD camera. The multi-dimensional tiff-file containing the entire video sequence was then imported into Matlab and cut into individual frames. For each frame, a region of interest of 23 × 23 μm^2 consisting of the trapping region was analyzed for fitting of the fluorescence peaks to 2D Gaussians. Since the fluorescence signal of a single molecule is very weak, the on-chip electron-multiplication gain was set to its maximum value, resulting in a signal amplification of approximately 1000 times[12].

5.4.2 Sample preparation for ssDNA

The setup used here for experiments is same as figure 5.1. The ssDNA solution consisted of an 8 nM solution of singly Cy3 labeled 600-nt ssDNA molecules in a TBE buffer consisting of 44 mmol L^{-1} Tris (tris(hydroxymethyl)aminomethane), 44 mmol L^{-1} boric acid, and 1 mmol L^{-1} EDTA (ethylenediaminetetraacetic acid). The solution is titrated to *p*H 8.5 with 1.0 mmol L^{-1} sodium hydroxide to ensure deprotonating the phosphodiester backbone, producing the maximum effective charge. Then the sample was placed on coverslip with 60:40 NiCr/AuPd with electrodes attached. A flow was induced for ssDNA to move on a coverslip for trapping.

5.4.3 Trapping ssDNA

A 600-nt ssDNA molecule was successfully trapped in a 10 µm corral trap; the experiments were done with help Christine Carlson. Figure 5.6 shows the successful trapping of a single 600nt ssDNA molecule in a corral trap. A trapping potential of -30 V was applied when a single ssDNA molecule had moved inside a corral trap. The molecule was observed in the center of the corral trap and remained centered due to the strong electrostatic potential well seen in figure 5.6B.Once the trapping potential is turned off, the ssDNA moves away from the center and out of the trap (Fig. 5.6C).Furthermore, it is conceivable that the observed fluorescence signal is stemming from two or more ssDNA molecules that are clustered together, which would explain the absence of fluorescence blinking as well as the observed higher fluorescence intensity. Blinking occurs namely because it is very unlikely that two or more molecules would switch to the “off” state at the exact same moment and for the same duration, so only intensity fluctuations will be observed.

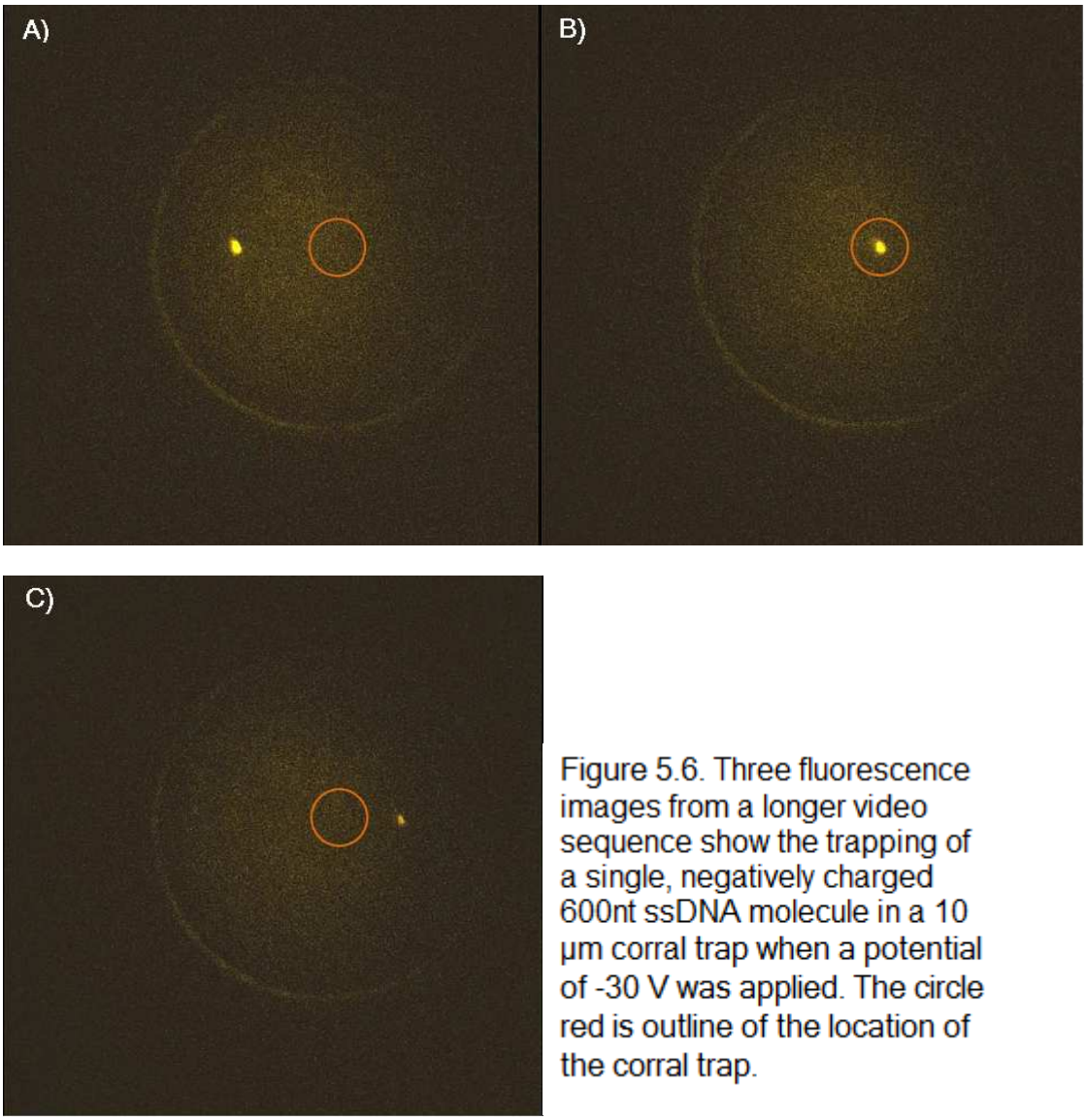

Figure 5.6. Three fluorescence images from a longer video sequence show the trapping of a single, negatively charged 600nt ssDNA molecule in a 10 μm corral trap when a potential of -30 V was applied. The circle red is outline of the location of the corral trap.

Chapter 6

Conclusion and Future Direction

6.1 Overall summery

The goal of research was to trap 600nt ssDNA in a corral trap, which I have successfully demonstrated with the help of Dr. Carlson. This technique allowed us to isolate and study single molecules in their native solution environment. Along this line, we wanted to introduce another ssDNA to the trapped molecule as well as study trapped molecules for longer times to understand their dynamics and/or interactions with binding partners. This research focused us to consider the fabrication of microfluidic devices with corral traps.

The intent of the thesis was to build electrostatic corral traps in microfluidic devices for trapping single molecules. In this thesis I have successfully fabricated a microfluidic devices that can be used in conjunction with corral traps. Microfluidic devices were fabricated by photolithography process using two different photoresists: a positive s1813 resist and a negative SU-8 resist. Both types of devices with integrated corral traps can be used for trapping and manipulating single molecules such as viruses, proteins, beads and DNA.

6.2 Future direction

The fabrication of electrostatic corral trap integrated in a microfluidic device has great benefits. Now, the experiments can go for longer period of time and flow of solution is easily established. Future experiments focuses on the trapping of 400, 200, 100 and 50 nt ssDNA using microfluidic and other ssDNA will be introduced to study how will they react with each other. Also, a different *p*H solution can be established and to study its influence on biomolecules. Also, not

just DNA, but viruses can potentially be trapped and studied. Future work is needed to improve the fabrication of corral traps using a photolithography process. So, that arrays of corral traps positioned across the channel can be fabricated in microfluidic devices. This will make trapping more efficient, allowing us to trap molecules in parallels in multiple corral traps at the same time.

References:

1. Ashkin, A.; Dziedzic, J. M.; Bjorkholm, J. E.; Chu, S., Observation of a single-beam gradient force optical trap for dielectric particles. *Opt. Lett.* **1986,** 11(5), 288 - 290.

2. Ashkin, A.; Dziedzic, J. M.; Yamane, T., Optical trapping and manipulation of single cells using infrared laser beams. *Nature* **1987,** 330(24), 769 - 771.

3. Finer, J. T.; Simmons, R. M.; Spudich, J. A., Single myosin molecule mechanics: piconewton forces and nanometre steps. *Nature***1994**, 368, 113 - 119.

4. Ashkin, A.; Dziedzic, J. M., Optical trapping and manipulation of viruses and bacteria. *Science* **1987,** 235, 1517 - 1520.

5. Ashkin, A.; Forces of a single-beam gradient laser trap on a dielectric sphere in the ray optics regime. *Biophys. J.* **1992,** 61, 569 - 582.

6. Optical Tweezers, “http://en.wikipedia.org/wiki/optical_tweezers”.

7. Ashkin, A., Trapping of atoms by resonance radiation pressure. *Phys. Rev. Lett.***1978,** 40 (12), 729 - 732.

8. Cohen, A. E.; Moerner, W. E., The anti-brownian electrophoretic Trap (ABEL Trap): fabrication and software. *Proc. SPIE*. **2005,** 5699, 296 - 306.

9. Carlson, C.; Sweeney, N.; Nasse, M.; Woehl, J., The corral trap: Fabrication and software development. *Proc. SPIE*. **2010,** 7571, 757108-1 - 6.

10. Carlson, C. (2010). *Development of the electrostatic corral for the trapping of single molecules in solution*, Chemistry. (Doctoral dissertation). Retrieved from ProQuest Dissertations and Theses.

11. Kuzyk, A.; Yurke, B.; Toppari, J.; Linko, V.; Torma, P., Dielectrophoretic trapping of DNA origami. *Small.***2008,** 4 (4), 447 – 450.
12. Terry, S.; Jerman, J.; Angell, B., A Gas Chromatographic Air Analyzer Fabricated on a Silicon Wafe. *IEEE Trans. Electron Devices.***1979,** 26 (12), 1880 – 1886.

13. Bassous, E.; Taub, H.; Kuhn, L., Ink jet printing nozzle arrays etched in Silicon. *Appl. Phys. Lett.* **1977,** 31, 135 – 137.

14. Gonzalez, A.; Hervas, M., Real sample analysis on microfluidic devices. *Talanta*. **2007,** 74, 342 – 357.

15. Sakamoto, C.; Nobuyasu, Y.; Yamada, M.; Nagase, H.; Seki, M.; Nasu, M., Rapid quantification of bacterial cells in portable water using a simplified microfluidic devices. *J. Microbiological Methods*. **2007,** 68, 643 – 647.

16. Stone, H.; Kim, S., Microfluidics: basic Issues, applications, and challenges. *AIChE J*. **2001,** 47, 1250 - 1254.

17. Bruzzone, A.; Costa, H.; Lonardo, P.; Lucca, D., Advances in engineered surfaces for functional performance. *CIRP Annals - Manufacturing Technology.* **2008,** 57, 750 – 769.

18. Ungerbock, B.; Mistlberger, G., Oxygen imaging in microfluidic devices with optical sensors applying color cameras. *Procedia Engineering*. **2010,** 5, 456 – 459.

19. Dragoi, V.; Cakmak, E.; Pabo, E., Metal wafer bonding for MEMS devices, *Romanian Journal of Information Science and Technology.***2010,** 13 (1), 65 – 72.

20. Moharana, M.; RaoPeela, N.; Khandekar, S., Distributed hydrogen production from ethanol in a microfuel processor. *Renewable and Sustainable Energy Reviews.***2011,** 15, 524 – 533.

21. Zhang, C.; Xing, D.; Li, Y., Micropumps, microvalves and micromixers for microfluidic chip: advances and trends. *J. Biotechnology Advances.***2007,** 25, 483 – 514.

22. Rogers, T.; Kowal, J., Selection of glass, anodic bonding conditions and material compatibility. *Sensors and Actuators B*. **2008,** 130, 436 – 448.

23. Chen, L.; Luo, G.; Liu, K.; Ma, J.; Yao, B., Bonding of glass based microfluidic chip at low or room temperature. *J. Sensors and Actuators B*. **2006,** 119, 335 – 344.

24. Fulton, T.; Dolan, G., Observation of single-electron charging effects in small tunnel junctions. *Physical Review Letters*. **1987,** 59 (1), 109 - 112.

25. Rolke, J., Nichrome Thin Film Technology and its application. *Electrocomponent Science and Technology.* **1981,** 9, 51 - 57.

26. Serway, R., *Principles of Physics* (2nd ed.). Fort Worth, Texas; London: Saunders College Pub. **1998**, p. 602.

27. Enderling, S.; Brown, C.; Smith, S.; Dick, M.; Stevenson, T.; Mitkova, M.; Kozicki, M.; Walton, A., Sheet resistance measurement of non-standard

cleanroom materials using suspended Greek cross test structures. **2006,** 19 (1), 2 – 9.

28. Chasteen, T., http://www.shsu.edu/chm_tgc/chemilumdir/JABLONSKI.html Sam Houston State University, Huntsville, Texas.

29. Davidson, M.; Abramowitz, M., Optical microscopy. *Encyclopedia of imaging science and technology*. **2002,** 2, 1106 - 1141.

30. Kamholz, A. E.; Schilling, E. A.; Yager, P., Optical measurement of transverse molecular diffusion in a microchannel. *Biophysical Journal*. **2001**, 80, 1967 - 1972.

31. Galambos, P. Ph.D. Thesis, Mechanical Engineering. University of Washington, Seattle (1998).

32. Weigl, B. H.; Yager, P., Silicon-microfabricated diffusion-based optical chemical sensor. *Sensors and Actuators B-Chemical*. **1997,** 39, 452 - 457.

33. Macounova, K.; Cabrera, C. R.; Holl, M. R.; Yager, P., Generation of natural pH gradients in microfluidic channels for use in isoelectric focusing. *Analytical Chemistry*. **2000,** 72, 3745 – 3751.

34. Duffy, D. C.; Gillis, H. L.; Lin, J.; Sheppard, N. F; Kellogg, G. J., Microfabricated centrifugal microfluidic systems: Characterization and multiple enzymatic assays. *Analytical Chemistry*. **1999,** 71, 4669 - 4678.

35. Sohn, L. L.; Saleh, O. A.; Facer, G. R.; Beavis, A. J.; Allan, R. S.; Notterman, D. A., Capacitance cytometry: Measuring biological cells one by one. *Proceedings of the National Academy of Sciences of the United States of America.***2000,** 97, 10687 - 10690.

36. Buchholz, B. A.; Doherty, E. A.; Albarghouthi, M. N.; Bogdan, F. M.; Zahn, J. M.; Barron, A. E., Microchannel DNA sequencing matrices with a thermally controlled "viscosity switch". *Analytical Chemistry.* **2001,** 73, 157 - 164.

37. Fan, Z. H.; Mangru, S.; Granzow, R.; Heaney, P.; Ho, W.; Dong, Q.; Kumar, R., Dynamic DNA hybridization on a chip using paramagnetic beads. *Analytical Chemistry.***1999,** 71, 4851 - 4859.

38. Koutny, L.; Schmalzing, D.; Salas-Solano, O.; El-Difrawy, S.; Adourian, A.; Buonocore, S.; Abbey, K.; McEwan, P.; Matsudaira, P.; Ehrlich, D., Eight hundred base sequencing in a microfabricated electrophoretic device. *Analytical Chemistry*. **2000,** 72, 3388 - 3391.

39. Lee, G. B.; Chen, S. H.; Huang, G. R.; Sung, W. C.; Lin, Y. H., Microfabricated plastic chips by hot embossing methods and their applications for DNA separation and detection. *Sensors and Actuators B-Chemical*. **2001,** 75, 142 - 148.

40. Glasgow, I. K.; Zeringue, H.C.; Beebe, D.J.; Choi, S.J.; Lyman, J.T.; Chan, N.G.; Wheeler, M.B., Handling individual mammalian embryos using microfluidics. *Ieee Transactions On Biomedical Engineering*. **2001,** 48, 570 - 578.

41. Yang, J.; Huang, Y.; Wang, X. B.; Becker, F. F.; Gascoyne, P. R., Cell separation on microfabricated electrodes using dielectrophoretic/gravitational field flow fractionation. *Analytical Chemistry*. **1999,** 71, 911 - 918.

42. Zondervan, R.; Kulzer, F.; Orlinskii, S. B.; Orrit, M., Photoblinking of Rhodamine 6G in Poly(vinyl alcohol): Radical Dark State Formed through the Triplet. *J. Phys. Chem. A.* **2003,** *107* (35), 6770-6776.

43. Walker, G.; Beebe, G., A passive pumping method for microfluidic devices. *The Royal Society of Chemistry.* **2002, 2**, 131-134.

44. Invitrogen, I. Fluorescence SpectraViewer. http://www.invitrogen.com/site/us/en/home/support/Research-Tools/Fluorescence-SpectraViewer.html.

45. Einstein, A.,On the movement of small particles suspended in stationary liquids required by the molecular-kinetic theory of heat.*Annalen der Physik.* **1905,** 17 (16), 549 - 560.

46. Jordá, E., Fantastic voyage.*Clinical and Translational Oncology.* **2009,** 11 (9), 561 - 563.